HOKKAIDO UNIVERSITY

Title	Establishment of a Method for Measuring the Heterogeneous Internal Structure of Polyelectrolyte Hydrogels Using Microelectrode Technique
Author(s)	西村, 拓哉
Degree Grantor	北海道大学
Degree Name	博士(ソフトマター科学)
Dissertation Number	甲第15794号
Issue Date	2024-03-25
DOI	https://doi.org/10.14943/doctoral.k15794
Doc URL	https://hdl.handle.net/2115/92283
Type	doctoral thesis
File Information	Takuya_Nishimura.pdf

Hokkaido University Collection of Scholarly and Academic Papers : HUSCAP

Doctoral Dissertation

Establishment of a Method for Measuring the Heterogeneous Internal Structure of Polyelectrolyte Hydrogels Using Microelectrode Technique

（微小電極法を用いた電解質ハイドロゲルの不均質内部構造測定法の構築）

Takuya Nishimura

Supervisor: Takayuki Kurokawa

HOKKAIDO
UNIVERSITY

Laboratory of Transformational Soft Matter

Graduate School of Life Science, Hokkaido University

Sapporo 001-0021, Japan

March 2024

Contents

Chapter 1 General Introduction

1.1 Overview

Hydrogels are formed from a three-dimensional polymer network with high affinity for water, allowing them to swell in water while maintaining their structure and retaining large amounts of water. Due to this characteristic, hydrogels exhibit excellent properties such as high flexibility, low friction, high biocompatibility, and stimulus responsiveness[1-5]. In particular, hydrogels with electrolytes in the polymer network are referred to as polyelectrolyte hydrogels, and they demonstrate swelling rates and electrical conductivity tens of times higher than those without electrolytes. These properties make them widely used in various applications such as absorbent materials for diapers and sanitary products, contact lenses[6], peptic ulcer agent[7], electrochemical cells[8], drug release control[9], and more.

In recent years, there has been successful improvement in addressing the brittleness traditionally associated with polyelectrolyte hydrogels, thanks to the double network concept involving the mutual infiltration of two types of polymer networks. This concept has enabled the flexible control of strength to a certain extent. The double network hydrogel (DN gel) demonstrating high strength and toughness, created under the concept mentioned, has been applied in various areas such as artificial cartilage[13] and gel 3D printing[14]. Polyelectrolyte hydrogels, which were once considered brittle and challenging to use materials, are now expected to find applications in a wider range of fields as new soft matter materials, thanks to the advancements brought about by this concept.

In considering the applications of such polyelectrolyte hydrogels, understanding the heterogeneity of the polymer network within the polyelectrolyte hydrogels is a crucial important[15]. This is because the heterogeneity of the polymer network inside the hydrogel introduces uneven dynamic behavior and energy states, becoming a significant factor that contributes to complex behaviors and properties in the liquid surrounding polymer network or polyelectrolyte hydrogel. Furthermore, in polyelectrolyte hydrogels, it is necessary to consider the influence of ions carrying charges on polyelectrolyte network[16]. Therefore, understanding the heterogeneity of the internal structure of the polyelectrolyte hydrogel and the distribution of charge density of the electrolyte polymer (referred to as polymer concentration) is essential. This knowledge serves as a guide for creating polyelectrolyte hydrogels that meet the required properties more precisely. It also contributes to improving fracture resistance and understanding the mechanisms involved. Hence, investigating the heterogeneity in polyelectrolyte hydrogels is indispensable.

Conventional methods for understanding the internal structure of polyelectrolyte hydrogels include scattering techniques using light or X-ray small-angle scattering[17-19], as well as microscopic observations using scanning electron microscopy (SEM) and transmission electron microscopy (TEM)[20,21], among others. Scattering techniques can reflect average information about the structure of electrolyte polymers in a narrow measurement region. Additionally, SEM and TEM allow for the acquisition of the distribution of electrolyte polymers in a two-dimensional plane by performing freeze-drying of polyelectrolyte hydrogels or staining of electrolyte polymers, followed by measuring their cross-sections.

However, it is believed that pre-treatments of polyelectrolyte hydrogels (such as staining or freezing) in these methods may introduce artifacts, causing transformations or damage to electrolyte polymers, and thus influencing the observed results. Even if the distribution of polyelectrolyte network spreading in three dimensions could be observed, it is challenging to

determine whether the results accurately and in real-time reflect the state of the network due to potential artifacts introduced during the observation process. As a result, there has been an urgent need to develop a method for spatial and in-situ measurements of the internal structure of polyelectrolyte hydrogels, but it has not been achieved due to the technical difficulties involved.

Amidst these challenges, in our laboratory, in 2016, we successfully adapted a microelectrode technique for measuring intracellular potential to hydrogels. This allowed us to measure the spatial distribution of polyelectrolyte network within polyelectrolyte hydrogels with a homogeneous internal structure[22,23]. This technique, which can measure the spatially the distribution of polyelectrolyte networks (internal structure) in small regions, was groundbreaking. However, at that time, it was difficult to accurately represent the internal structure of polyelectrolyte hydrogels with heterogeneity due to spatial resolution limitations. Therefore, the main focus of this dissertation is to enhance the microelectrode technique and establish a method for measuring the heterogeneous internal structure of polyelectrolyte hydrogels.

Firstly, I enhanced the hardware resolution of this method to evaluate the detailed structure of the network. Subsequently, using the improved technique, I verified whether it is possible to measure the electric potential of polyelectrolyte hydrogels locally and continuously with heterogeneous internal structures. In doing so, I established a method for spatial and in-situ measurements of the internal structure of polyelectrolyte hydrogels. As a result, I accomplished the measurement of heterogeneous structures at the sub-micrometer scale using the microelectrode technique. Furthermore, as an applied validation of this method, I observed the internal structure of phase-separated hydrogels with irregular and unknown-scale

heterogeneous structures, distinct from P-DN. Additionally, through the observation of the internal structure of the polyelectrolyte network in the damage zone of DN gels, which was challenging using conventional methods, I speculated on a fracture pattern based on the sacrificial bonding principle.

1.2 Outline of this dissertation

In Chapter 2, I introduce the heterogeneity of hydrogels and the fundamental knowledge of polyelectrolyte hydrogels. Following this, I provide a summary of conventional methods for measuring the internal structure of polyelectrolyte hydrogels. Additionally, I discuss the preceding research on the microelectrode technique, which has been considered as a potential and advanced method for internal structure measurements of the polyelectrolyte hydrogels.

In Chapter 3, I discuss methods to enhance the spatial resolution of the device for analyzing the structure of heterogeneous polyelectrolyte hydrogels. Specifically, I provide an overview of the device system, describe noise processing/removal methods, and explore considerations for achieving a temperature-controlled system with the aim of expanding the measurement range.

In Chapter 4, I verify the capability of the improved microelectrode technique to measure the heterogeneous internal structure of electrolyte hydrogels up to a certain scale. Specifically, I use electrolyte microparticle DN gels, which encapsulate electrolyte microparticle gels with known scales, as model materials. I conduct electric potential measurements using the microelectrode technique on these gels. By comparing the results with the sizes of the electrolyte microparticle gels obtained from microscopic images, I evaluate the tracking capability of the microelectrode technique for heterogeneous structures.

In Chapter 5, I conducted internal structure measurements of electrolyte hydrogels with indefinite and unknown-scale heterogeneity, unlike P-DN, to confirm the utility of the improved microelectrode technique. Specifically, I conducted electric potential measurements on phase

separated DN gels with a structure where polyelectrolyte network undergoes phase separation and then converted the results to polymer concentration profiles. I confirmed the spatial distribution of the inferred polymer electrolyte network from the results and checked if it aligned with the tendencies of phase separation. Furthermore, by verifying the tracking capability of the aggregation structure sizes obtained from polymer concentration profiles, I aimed to estimate the spatial resolution of the improved microelectrode technique more accurately.

In Chapter 6, leveraging the improved microelectrode technique, I conducted observations of the internal structure of polyelectrolyte network in the damage zone of DN gels. This was an aspect that conventional measurement methods could not achieve, so I aimed to infer the fracture patterns based on the sacrificial bonding principle of DN gels. Specifically, by measuring the electric potential at regular intervals from the crack tip in the damage zone formed by tearing the DN gel, I observed and visualized the structure of the electrolyte network in the damage zone. Furthermore, I aimed to elucidate the spatial fracture patterns of the polyelectrolyte network based on the changes in their structure according to the sacrificial bonding principle.

Concluding remarks are summarized in **Chapter 7**.

1.3 References

1. S. Ma, M. Scaraggi, D. Wang, X. Wang, Y. Liang, W. Liu D. Dini & F. Zhou, *Adv. Funct. Mater* **2015***,* 25, 7366.
2. P. Li, Y. F. Poon, W. Li, H. Y. Zhu, S. H. Yeap, Y. Cao, X. Qi, C. Zhou, M. Lamrani, R. W. Beuerman, E. T. Kang, Y. Mu, C. M. Li, M. W. Chang, S. S. J. Leong & M. B. Chan-Park, *Nat. Matter* **2011***,* 10, 149.
3. I. Tokarev & S. Minko, *Soft Matter* **2009***,* 5, 511.
4. M. C. Branco, D. J. Pochan, N. J. Wagner & J. P. Schneider, *Biomaterials* **2010***,* 31, 9527.
5. Gong, J. P.; Kurokawa, T.; Narita, T.; Kagata, G.; Osada, Y.; Nishimura, G.; Kinjo, M. Synthesis of Hydrogels with Extremely Low Surface Friction. *Journal of the American Chemical Society* **2001**, 5582–5583.
6. Newman, J. P.; Koch, J.; Goode, R. L., Closed dressings after laser skin resurfacing. *Archives of Otolaryngology-Head & Neck Surgery* **1998,** *124* (7), 751-757.
7. Humphreys ER & Triffitt JT, *Nature* **1968**,219,1173-1173
8. Tiyapiboonchaiya, C.; Pringle, J. M.; Sun, J. Z.; Byrne, N.; Howlett, P. C.; Macfarlane, D. R.; Forsyth, M., The zwitterion effect in high-conductivity polyelectrolyte materials. *Nat Mater* **2004,** *3* (1), 29-32.
9. Kikuchi, A.; Okano, T., Pulsatile drug release control using hydrogels. *Adv Drug Deliver Rev* **2002,** *54* (1), 53-77.
10. Gong, J. P.; Katsuyama, Y.; Kurokawa, T.; Osada, Y. Double- Network Hydrogels with Extremely High Mechanical Strength. *Adv. Mater.* **2003**, 15, 1155−1158.
11. Yasuda, K.; Gong, J. P.; Katsuyama, Y.; Nakayama, A.; Tanabe, Y.; Kondo, E.; Ueno, M.; Osada, Y. Biomechanical Properties of High-Toughness Double Network Hydrogels. *Biomaterials* **2005**, *26* (21), 4468–4475.

12. Gong, J. P. Why are double network hydrogels so tough? . *Soft Matter* **2010**, 6, 2583−2590.

13. Azuma, C.; Yasuda, K.; Tanabe, Y.; Taniguro, H.; Kanaya, F.; Nakayama, A.; Yong, M. C.; Jian, P. G.; Osada, Y. Biodegradation of High-Toughness Double Network Hydrogels as Potential Materials for Artificial Cartilage. *Journal of Biomedical Materials Research - Part A* **2007**, *81* (2), 373–380.

14. R. Hidema ,; K. Sugita, ; H. Furukawa. 3-Dimensional Freeform Fabrication of High-Strength Gels by Laser Scanning Irradiation *Trans. J. Soc. Mech. Eng. (A)* **2011**, 77, 1002-1006

15. Shibayama, M. Spatial inhomogeneity and dynamic fluctuations of polymer gels. *Macromolecular Chemistry and Physics* **1998**, 199 (1).

16. K.デュセック,;柴山光弘,;浦山健治.ゲルの科学,講談社 **2020**

17. Shibayama, M., Ikkai, F., Shiwa, Y., Rabin, Y. Effect of degree of cross-linking on spatial inhomogeneity in charged gels .1. Theoretical predictions and light scattering study. *Journal of Chemical Physics* **1997**, 107(13) 5227-5235

18. Nakajima, T.; Kurokawa, T.; Ahmed, S.; Wu, W.-L.; Gong, J. P. Characterization of internal fracture process of double network hydrogels under uniaxial elongation. *Soft Matter* **2013**, 9, 1955−1966.

19. Fukao, K.; Nakajima, T.; Nonoyama, T.; Kurokawa, T.; Kawai, T.; Gong, J. P. Effect of relative strength of two networks on the internal fracture process of double network

hydrogels as revealed by in situ small-angle X-ray scattering. *Macromolecules* **2020**, 53, 1154−1163.

20. Cascone, M. G.; Lazzeri, L.; Sparvoli, E.; Scatena, M.; Serino, L. P.; Danti, S. Morphological Evaluation of Bioartificial Hydrogels as Potential Tissue Engineering Scaffolds. *Journal of Materials Science: Materials in Medicine* **2004**, *15* (12), 1309–1313.
21. Kiyama, R.; Yoshida, M.; Nonoyama, T.; Tomas, S.; Jinnai, H.; Kurokawa, T.; Nakajima, T.; Gong, J. P. Nanoscale TEM Imaging of Hydrogel Network Architecture, *Advanced Materials* **2022**, 2208902-2208902
22. Guo, H.; Kurokawa, T.; Takahata, M.; Hong, W.; Katsuyama, Y.; Luo, F.; Ahmed, J.; Nakajima, T.; Nonoyama, T.; Gong, J. P. Quantitative Observation of Electric Potential Distribution of Brittle Polyelectrolyte Hydrogels Using Microelectrode Technique. *Macromolecules* **2016**, *49* (8), 3100–3108.
23. Guo, H.; Hong, W.; Kurokawa, T.; Matsuda, T.; Wu, Z. L.; Nakajima, T.; Takahata, M.; Sun, T.; Rao, P.; Gong, J. P. Internal Damage Evolution in Double-Network Hydrogels Studied by Microelectrode Technique. *Macromolecules* **2019**, *52* (18), 7114–7122.

Chapter 2 Background

2.1 General consideration of hydrogels

2.1.1 Hydrogels

The gel is defined as "a polymer and its swollen form with a three-dimensional network structure insoluble in any solvent"[1]. Common examples include jelly, konjac, and contact lenses. Gels swell depending on the solvent, and the type of gel varies with the medium. Those with water as the solvent are specifically called “hydrogel.” Hydrogels' crosslinking structures can be classified into chemical crosslinking and physical crosslinking. Chemical crosslinking involves the formation of crosslinking structures through chemical reactions. On the other hand, physical crosslinking occurs through hydrogen bonds, ion bonds, or entanglement of polymer chains.

Moreover, despite being mostly composed of a solvent, hydrogels behave as solids due to the contribution of a few percent in weight from the polymer network. At the same time, when observed at a microscopic level, hydrogels also display polymer solution-like properties. These unique characteristics enable them to retain amounts of solvent up to a thousand times their polymer weight, exhibit more than tenfold deformability, and accommodate or allow the passage of large molecules like proteins or small molecules.

2.1.2 Hydrogel heterogeneity

Hydrogels contain crosslinks of polymer chains, and in the case of chemically crosslinked hydrogels, these are formed during synthesis through the reaction between monomers and crosslinking agents. Generally, crosslinking points are formed at random positions within the hydrogel, and the chain length of the polymer connecting the crosslinking points is not uniform. Therefore, during the synthesis process, variations in the density and entanglement of the

network structure occur. This heterogeneity associated with crosslinking is referred to as the "hydrogel heterogeneity." In particular, the crosslinking in chemical hydrogels, unlike physical hydrogels, is believed to have a significant impact on the properties of chemical gels because it does not undergo dissolution, unraveling, or rearrangement. Generally, the heterogeneity of hydrogels can be classified into four types, as shown in Figure 2.1: (i) spatial heterogeneity, (ii) topological heterogeneity, (iii) bonding heterogeneity, and (iv) mobility heterogeneity[2].

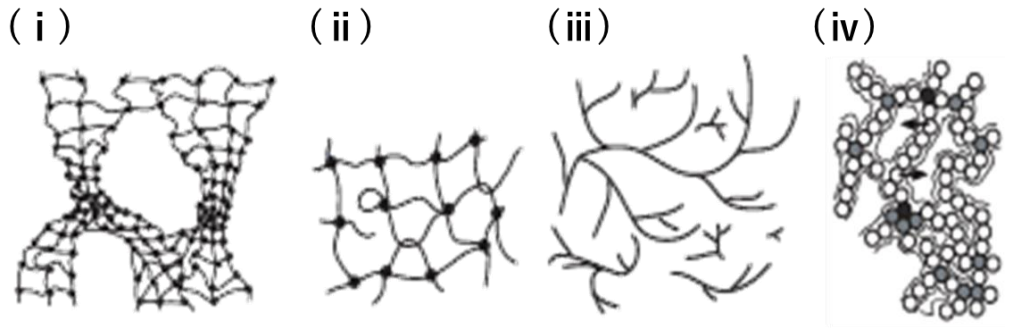

Fig. 2.1 The heterogeneity of hydrogels. (i) spatial heterogeneity, (ii) topological heterogeneity, (iii) bonding heterogeneity, and (iv) mobility heterogeneity[2].

2.1.3 Polyelectrolyte hydrogels

Polyelectrolyte hydrogel is a hydrogel composed of polyelectrolyte network with charged macroions and counterions dispersed in the solution. This hydrogel, influenced by the impact of macroions fixed to the polyelectrolyte network, exhibits heterogeneities such as phase-separated structures, in addition to the heterogeneity introduced in 2.1.2. Furthermore, polyelectrolyte hydrogels demonstrate unique characteristics, including counterion condensation[3,4], the formation of electric double layers[5], and a high swelling ratio.

(1) Counterion condensation in polyelectrolyte hydrogels

In the highly ionized macroions within the polyelectrolyte hydrogel, a strong electrostatic interaction occurs with the surrounding counterions. In other words, counterions localize around the polyelectrolyte main chain, significantly reducing its activity. This phenomenon is referred to as ion condensation. Of course, there is a density limit for the presence of ions within the polyelectrolyte hydrogel, so there is a limit to the ionization of the polyelectrolyte main chain, and not all counterions will localize. The electrostatic potential of counterion condensation is represented by the Manning parameter in the following equation(2.1)[3]:

$$\xi = \frac{z^2 e^2}{4\pi DTbk_b} \quad (2.1)$$

Here, z is ion valence, e is electric coefficient, D is dielectric constant, T is absolute temperature, b is Average distance between adjacent ionic groups on the electrolyte polymer chain, k_b is Boltzmann's constant.

It is known that the system adopts a stable state when ξ=1 and becomes unstable when $\xi \geq 1$. In this case, macroions and counterions undergo ion condensation, resulting in an increase

in the average distance *b* between adjacent ionized groups on the effective electrolyte polymer. This leads to ξ reaching 1, signifying a stable state.。

(2) Activity and activity coefficient

In the polyelectrolyte hydrogel, electrolyte polymer chains connected at crosslinking points are intertwined in a three-dimensional network. There exist co-ions with the same charge as the fixed macroion on the polymer chain and counterions with opposite charges, as shown in Figure 2.2[4]. Due to the strong influence of the macroion, counterions can be classified into two types: (ⅰ) the counterion restricted in the vicinity of the macroion and (ⅱ) the counterion that can move freely around the Debye length range of macroion. In the polyelectrolyte hydrogel, some counterions are fixed to the macroion, causing a deviation from the ideal state in the thermodynamic behavior of ions. Therefore, the concentration of ions in the real state is expressed in terms of activity, accounting for the deviation from the ideal state.

Here, the counterions that influence the thermodynamic phenomena within the hydrogel are those that can move freely : counterions (ⅱ). The activity of the counterions corresponds to the concentration of effective counterions (ⅱ), and the activity coefficient of the counterions corresponds to ratio of the activity of the counterions with respect to the total counterion concentration. The correction factor for this deviation is referred to as the activity coefficient[6].

$$\gamma_i = \frac{a_i}{C_i} \quad (2.2)$$

Here, γ_i is activity coefficient of ions, a_i is activity of ions, C_i is molar concentration of ions.

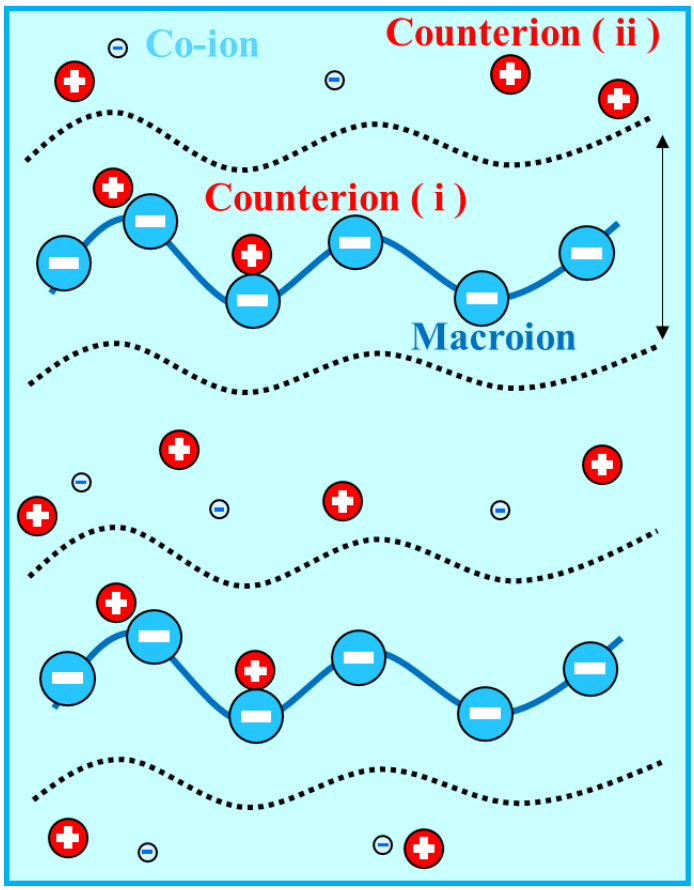

Fig. 2.2 Conceptual diagram of various ions in a polyelectrolyte hydrogel.

(3) Formation of electric double layer and Donnan potential of polyelectrolyte hydrogels

When a polyelectrolyte hydrogel with fixed macroions is immersed in an electrolyte solution, at the surface of the polyelectrolyte hydrogel, co-ions with the same charge as the macroions are repelled, while counterions with opposite charges are attracted. The electrical neutrality is maintained inside the polyelectrolyte hydrogel and the electrolyte solution. However, due to the competition between electrostatic interactions and ion diffusion, near the surface of the polyelectrolyte hydrogel, small regions called the electric double layer are formed, where positive and negative charges are separated. This equilibrium state is called the Donnan equilibrium, and the electric potential difference generated at this time is called the Donnan potential[7] (Figure 2.3). Here, Donnan equilibrium is continuously maintained within the hydrogel.

In general, when impermeable ions (macroions) and permeable ions are present across a semipermeable membrane, the counterions of macroions tend to localize around the macroions, leading to the formation of an asymmetric ion concentration distribution across the semipermeable membrane and the generation of a Donnan potential. In the case of polyelectrolyte hydrogels, the electrical double layer near the surface of the polyelectrolyte hydrogel exhibits an asymmetric ion concentration distribution. Consequently, a Donnan potential is generated between the polyelectrolyte hydrogel and the electrolyte solution in a manner similar to the semipermeable membrane.

The Donnan potential in the polyelectrolyte hydrogel is derived by considering the effective ion equilibrium inside and outside the polyelectrolyte hydrogel. The electrochemical potentials of effective counterions and co-ions on the macroion side, as illustrated in Figure 2.3, are expressed as follows:

$$\bar{\mu}_i = \mu_i^0 + RT\ ln\ a_{i,g} + \pi\bar{V}_i + z_i F\Phi_g \quad (2.3)$$

Here $\bar{\mu}_i$ is electrochemical potential, μ_i^0 is standard electrochemical potential, $a_{i,g}$ is the activity of ions in the polyelectrolyte hydrogel, $\pi\bar{V}_i$ is the osmotic pressure of water flows from the solution side of membrane to macroion side, Φ_g is the electric potential in the polyelectrolyte hydrogel.

In order for this to be in equilibrium with the electrical potential $\bar{\mu}_i'$ of the counterions and co-ions in the external electrolyte solution, the following relationship must hold.

$$\bar{\mu}_i = \bar{\mu}_i' \rightleftarrows \mu_i^0 + RT\ ln\ a_{i,g} + \pi\bar{V}_i + z_i F\Phi_g = \mu_i^{0\prime} + RT\ ln\ a_{i,s} + z_i F\Phi_s \quad (2.4)$$

Here $\bar{\mu}_i'$ is electrochemical potential in electrolyte solution, $a_{i,s}$ is the activity of ions in the electrolyte solution, Φ_s is the electric potential in the electrolyte solution.

As a result, the following equation holds, and this potential difference $\Delta\Phi$ is called the Donnan potential Φ_D[8].

$$\Delta\Phi = \Phi_s - \Phi_g = \frac{RT}{z_i F}\ln\left(\frac{a_{i,g}}{a_{i,s}}\right) + \frac{\pi\bar{V}_i}{z_i F} = \Phi_D \quad (2.5)$$

In general, since $\frac{RT}{z_i F}\ln\left(\frac{a_i}{a_i'}\right) \gg \frac{\pi\bar{V}_i}{z_i F}$, the Donnan potential $\Delta\Phi$ in this dissertation is expressed by the following equation, neglecting the second term.

$$\Phi_D = \frac{RT}{z_i F}\ln\left(\frac{a_{i,s}}{a_{i,g}}\right) = \frac{RT}{z_i F}\ln\left(\frac{\gamma C_{i,s}}{\gamma' C_{i,g}}\right) \quad (2.6)$$

Here $C_{i,g}$ is molar concentration of ions in the polyelectrolyte hydrogel, $C_{i,s}$ is molar concentration of ions in the electrolyte solution, $a_{i,g}$ is the activity of ions in the polyelectrolyte hydrogel, $a_{i,s}$ is the activity of ions in the electrolyte solution, γ is the activity coefficient of ions in the electrolyte solution, γ' is the activity coefficient of ions in the polyelectrolyte hydrogel.

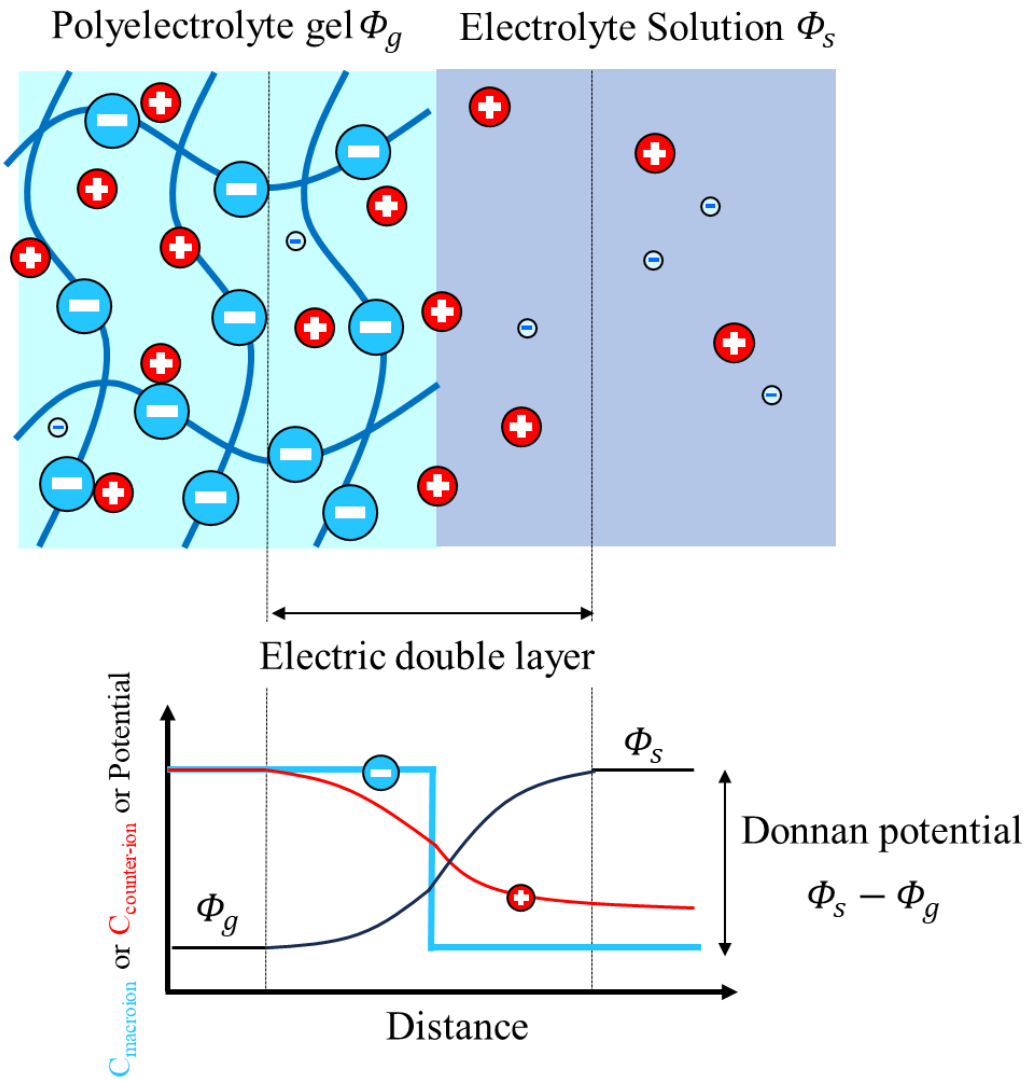

Fig. 2.3 Illustration of the electric double layer formed near the interface between the negatively charged macroion-containing polyelectrolyte hydrogel and the electrolyte solution, depicting the resulting asymmetric distribution of ions and the Donnan potential.

(4) Swelling and osmotic pressure of polyelectrolyte hydrogels

The unique swelling behavior of polyelectrolyte hydrogels is determined by the osmotic pressure exerted on the hydrogel. The total osmotic pressure (Π_{total}) of the polyelectrolyte hydrogel is the sum of three osmotic pressure components: the osmotic pressure derived from the rubber elasticity of the polymer (Π_{el}), the osmotic pressure derived from the mixing of polymer and solvent (Π_{mix}), and the osmotic pressure specific to the counterions in the polyelectrolyte hydrogel (Π_{ion})[9].

$$\Pi_{total} = \Pi_{el} + \Pi_{mix} + \Pi_{ion} \quad (2.7)$$

Osmotic pressure derived from rubber elasticity of polymers（Π_{el}）: In a certain state, the polymer adopts a suitable expanded spherical form. In this state, when the polymer is pulled by both ends, it tends to contract, and when pushed, it tends to expand. At this point, pressure due to rubber elasticity is generated. Π_{el} is given by the rubber elasticity theory as follows.

$$\Pi_{el} = \frac{n_p k_b T}{V_{as-pre}} \left[\frac{p}{2p_0} - \left(\frac{p}{p_0} \right)^{\frac{1}{3}} \right] \quad (2.8)$$

Here n_p is the number of polymer chains, V_{as-pre} is the volume of as-prepared gels, p is the volume fraction of polymer chains after swelling, p_0 is the volume fraction of polymer chains with as-prepared state.

Osmotic pressure derived from the mixing of polymer and solvent（Π_{mix}）: In a polymer-friendly liquid environment (where the bridging point is absent, and the polymer dissolves), the polymer is surrounded by the liquid, causing pressure in the direction of polymer expansion. Π_{mix} is determined by the Flory-Huggins equation.

$$\Pi_{mix} = -\frac{RT}{V_1}[in(1-p) + p + \chi p^2] \quad (2.9)$$

Here, V_1 is the molar volume of the solvent, χ is the thermodynamic interaction parameter between polymer and solvent.

Osmotic pressure derived from counter ions (Π_{ion})：It is specific to charged polyelectrolyte hydrogels and corresponds to the difference between the mobile ions in the polyelectrolyte hydrogel and those in the solvent. The pressure is generated in the direction of swelling the gel as the counterions move within the gel.

$$\Pi_{ion} = RT\sum_{i=1}^{N}(C_i^{gel} - C_i^{solvent}) \quad (2.10)$$

Here, C_i^{gel} and $C_i^{solvent}$ are the concentration of the ions in the hydrogel and solvent.

By combining these three osmotic pressure terms, the total osmotic pressure (Π_{total}) of the polyelectrolyte hydrogel can be obtained.

$$\Pi_{total} = \frac{n_p k_b T}{V_{as-pre}}\left[\frac{p}{2p_0} - \left(\frac{p}{p_0}\right)^{\frac{1}{3}}\right] - \frac{RT}{V_1}[in(1-p) + p + \chi p^2] + RT\sum_{i=1}^{N}(C_i^{gel} - C_i^{solvemt}) \quad (2.11)$$

Now, using the volume fractions of the polymer denoted by p and p_0, the swelling ratio Q can be expressed as follows.

$$\frac{p}{p_0} = \frac{V_p/V_{swelled}}{V_p/V_{as-pre}} = \frac{1}{Q} \quad (2.12)$$

Here, p is the volume fraction of the polymer in the swelling polyelectrolyte hydrogel, p_0 is the volume fraction of the polymer before the swelling.

Furthermore, Π_{total} is zero at equilibrium, and the Π_{mix} term can be ignored. Therefore, the relationship between the swelling ratio Q and osmotic pressure is expressed as follows.

$$\Pi_{total} = \frac{n_p k_b T}{V_{as-pre}} \left[\frac{1}{2Q} - \left(\frac{1}{Q} \right)^{\frac{1}{3}} \right] + RT \sum_{i=1}^{N} (C_i^{gel} - C_i^{solvemt}) \approx 0 \quad (2.13)$$

2.1.4 Double network hydrogel (DN gel)

Polyelectrolyte hydrogels possess excellent properties but suffer from being hard and brittle, making them less suitable for use as materials or components. Addressing this challenge, Gong et al. developed a Double Network Hydrogel (DN gel) where the first network consists of hard and brittle polyelectrolyte network, and the second network comprises soft and highly stretchable non- polyelectrolyte network, creating a mutually infiltrating network structure of the two polymer chains[10, 11]. When the DN gel is destructed, the hard first network within the DN gel is ruptured preferentially, while the soft second network maintains its structure, preventing macroscopic fracture. As a result, it becomes an exceptionally strong and tough gel. This principle is known as “sacrificial bond theory” and has garnered recent attention for its possibility application in enhancing the strength of various hydrogels[12-15].

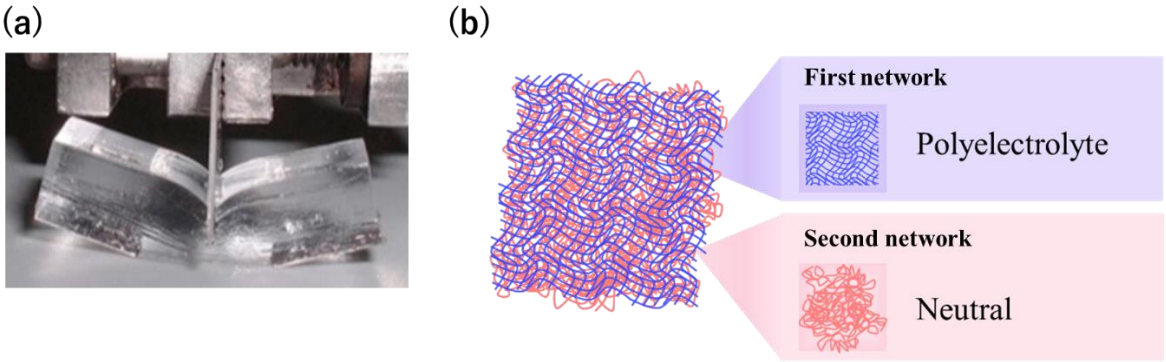

Fig. 2.4 (a) A photograph illustrating the toughness of the DN gel[12]. (b) An illustration depicting the network structure of the DN gel.

2.2 Conventional structural analysis methods in polyelectrolyte hydrogels

The conventional methods for structural analysis of polyelectrolyte hydrogels include scattering techniques for internal structure measurement and microscopy for surface structure observation.

Scattering methods for structural analysis involve irradiating polyelectrolyte hydrogels with electromagnetic waves such as light or X-rays, as well as particle beams like neutrons. By analyzing the scattering patterns resulting from the irradiation, the structure of the polyelectrolyte hydrogel can be estimated based on the scattering states related to cross-linking within the polyelectrolyte hydrogel[16-18]. In scattering methods, it is possible to measure the size of the polymer network and microgel within the polyelectrolyte hydrogel by considering the average values within the beam irradiation range. The resolution of this method ranges from 1 nm to 1 μm.

Structural measurements using microscopy techniques involve the use of scanning electron microscopy (SEM), transmission electron microscopy (TEM), and atomic force microscopy (AFM). SEM and TEM methods observe the surface or cross-section of the polyelectrolyte hydrogel by freezing and drying or performing iron staining of the polymer chains[19,20]. AFM is a technique that involves bringing the tip of a cantilever probe into contact with the polyelectrolyte hydrogel to observe and measure surface structures and elasticity[21]. AFM can measure polyelectrolyte hydrogels in ambient conditions, but the measurement range is very localized. The resolution in microscopy techniques is typically in the range of approximately 1 nm to 1 μm.

However, with these methods, observing the distribution of polymer networks that spread in three dimensions is challenging. Especially for gaining detailed insights into the internal structure of polyelectrolyte hydrogels with heterogeneous structures, it is necessary to develop techniques that allow spatial and in-situ measurements with a high spatial resolution, in place of scattering and microscopy methods.

2.3 Internal structure analysis by Donnan potential measurement

2.3.1 Microelectrode technique (MET)

In polymer research, the microelectrode technique is employed by adapting it to polyelectrolyte hydrogels to measure the Donnan potential as the difference in activity between ions around the macroions fixed to the electrolyte polymer chains inside the polyelectrolyte hydrogel and ions in the electrolyte solution. This is due to the establishment of Donnan equilibrium by small ions. Within the interior of the polyelectrolyte hydrogel, the concentration of counterions is significantly higher than that of co-ions. Therefore, by focusing on the counterions, it becomes easier to discuss the state of macroions in the polyelectrolyte network.

In the microelectrode technique, a low-concentration electrolyte solution is used as the reference solution, and it consists of a reference electrode fixed in the reference solution and a capillary (microelectrode) inserted into the interior of the polyelectrolyte hydrogel. Following the method of measuring cellular potentials, a stable electrode (such as a carbon electrode) is used as the reference electrode, and a capillary is created using a glass tube with a tip diameter ranging from several hundred nanometers to several micrometers. This capillary is filled with an Ag/AgCl electrode and a high-concentration potassium chloride solution (KCl_{aq}).

It is believed that the tiny leakage range of the KCl_{aq} at the tip of the capillary is within the detection range of the microelectrode (at least the size of the capillary diameter). When the detection range penetrates into the polyelectrolyte hydrogel, changes in the concentration of counterions around the macroion result in variations in chloride ion concentration near the Ag/AgCl electrode, indicating redox reactions.

Oxidation : $Ag + Cl^- - e^- \rightleftarrows AgCl$ (2.14)

Reduction : $AgCl + e^- \rightleftarrows Ag + Cl^-$ (2.15)

The electric potential difference obtained by subtracting the electric potential detected at the reference electrode from the electric potential generated by this redox reaction is the Donnan potential between the polyelectrolyte hydrogel and the reference solution.

$$\Delta\Phi_D = \Phi_{ele} - \Phi_{ref} \quad (2.16)$$

Here, it is necessary to consider the electrode potential between the reference electrode and the Ag/AgCl electrode, the electrode potential between the high-concentration KCl_{aq} inside the capillary and the Ag/AgCl electrode, the electrode potential between the electrolyte solution and the reference electrode, and the liquid-junction potential generated between the high-concentration KCl_{aq} inside the capillary and the polyelectrolyte hydrogel.

The electrode potential between the reference electrode and the Ag/AgCl electrode can be ignored during measurements by performing an offset of the potential at the stage when the capillary is immersed in the reference solution (before insertion into the polyelectrolyte hydrogel) and setting that value to 0 mV. The electrode potential between the high-concentration KCl_{aq} inside the capillary and the Ag/AgCl electrode, as well as the electrode potential between the electrolyte solution and the reference electrode, can be theoretically minimized by using ideal non-polarizable electrodes such as Ag/AgCl electrode or carbon electrodes. Additionally, performing an offset can further allow these potentials to be ignored during measurements. The liquid-junction potential occurring between the high-concentration KCl_{aq} and the polyelectrolyte hydrogel can be minimized to an extremely small value due to

the high-concentration KCl_{aq} acting as a salt bridge. Therefore, it is possible to ignore this electric potential during measurements. In summary, if the influence of the disruption of the polyelectrolyte hydrogel by the capillary is eliminated, the electric potential measured by the microelectrode technique becomes the Donnan potential generated by the counterions of the polyelectrolyte hydrogel and the counterions of the reference electrolyte solution. This electric potential is calculated from the average counterion activity within the detection range at the tip of the capillary and the counterion activity of the electrolyte solution.

Figure 2.5 illustrates the apparatus system of the microelectrode technique used in our laboratory. A carbon electrode is employed as the reference electrode. The capillary is created by placing an Ag/AgCl electrode and 3 M KCl_{aq} in a glass tube. The capillary is fixed to an electric micro-manipulator (DMA-1511, Narishige, Japan), allowing for high-precision and speed control. Consequently, by advancing the capillary while locally disrupting the hydrogel, it is possible to obtain a continuous Donnan potential between the polyelectrolyte hydrogel and the reference solution along the direction of capillary progression. Therefore, the microelectrode technique allows for obtaining the Donnan potential distribution in the polyelectrolyte hydrogel along the direction of capillary progression without the need for pre-treating the polyelectrolyte hydrogel.

The Figure 2.6 illustrates an example of the electric potential profile when using microelectrode techniques to insert a negatively charged polyelectrolyte hydrogel. When the capillary is in the reference solution, there is minimal detection of electric potential difference (①). However, as the capillary approaches the gel, the potential begins to decrease, and upon

insertion into the polyelectrolyte hydrogel (②), it becomes possible to detect the Donnan potential between the polyelectrolyte hydrogel and the reference solution as electric difference (③).Here, the vertical axis represents the electric potential, and the horizontal axis represents the distance advanced by the capillary.

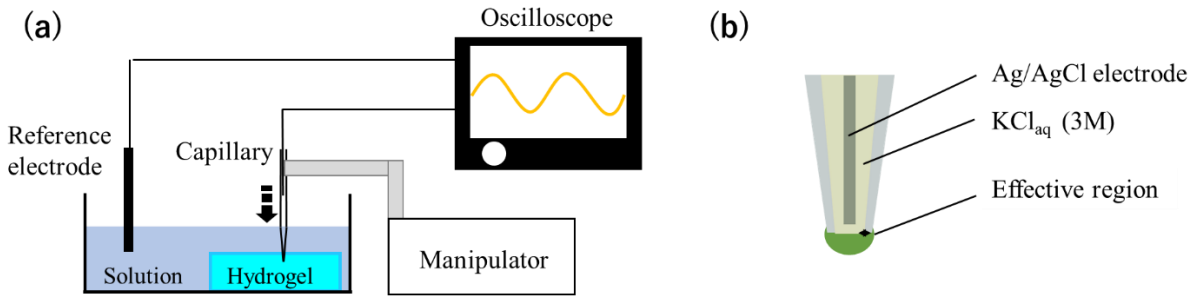

Fig. 2.5 (a) Schematic diagram of the microelectrode technique. The capillary is fixed to the manipulator and can be controlled at speeds of 0.16 μm/s or higher. (b) Schematic diagram of the capillary.

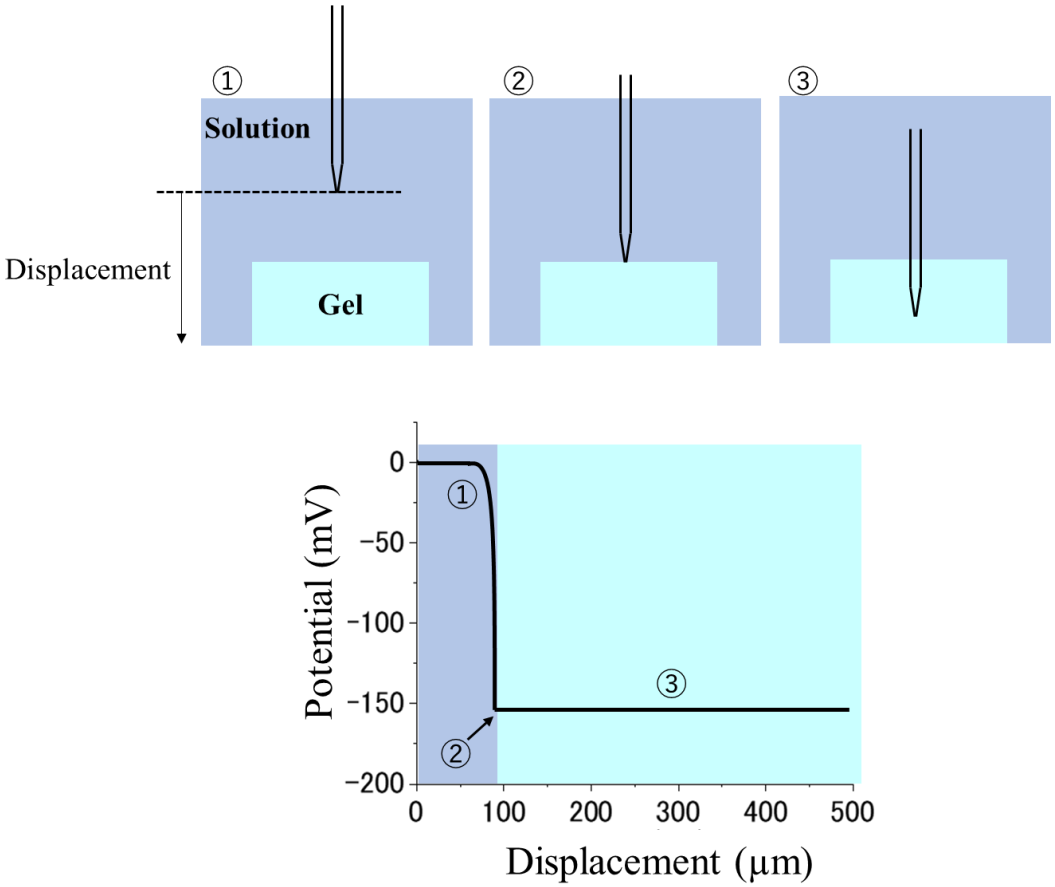

Fig. 2.6 Example of a potential profile obtained by microelectrode technique when measuring a negatively charged polyelectrolyte hydrogel. The vertical axis represents the electric potential, and the horizontal axis represents the distance advanced by the capillary.

2.3.2 Previous studies measuring internal structure of polyelectrolyte hydrogels by microelectrode technique

Rainer et al. were the first to apply microelectrode techniques to polyelectrolyte hydrogels[28]. They discovered that when applying an electric field to the polyelectrolyte hydrogel, the Donnan potential differed between the inflow and outflow regions of the electric field. Furthermore, they found a correlation between changes in this Donnan potential and the swelling or deswelling of the hydrogel. Blyakhman et al. measured the differences in the activity of effective counterions to ions within the polyelectrolyte hydrogel when altering the concentration of the reference solution[29]. From this, they discovered that the factor causing the contraction of the polyelectrolyte hydrogel is a decrease in the activity of effective counterions, which also leads to a decrease in osmotic pressure.

Microelectrode techniques have been applied to hydrogels, and measurements of activity have provided valuable insights. In response to these achievements, Guo et al. utilized microelectrode techniques to infer the internal structure of polyelectrolyte hydrogels[30,31]. Guo et al. initially validated the impact of capillary-induced disruption of the polyelectrolyte hydrogel on electric potential measurements using microelectrode techniques[30]. They varied conditions such as the tip diameter, wall thickness of the capillary and the insertion speed of the electrode, and measured the electric potential of fragile polyelectrolyte hydrogels prone to disruption by electrode insertion. As a result, it was found that the electric potential remains constant regardless of the insertion rate, but when the tip diameter and wall thickness of the capillary increase, the electric potential decreases exponentially. Moreover, it was discovered that with electrodes having a wall thickness smaller than the local Debye length around the

capillary, it is possible to disregard the impact of polyelectrolyte hydrogel disruption, resulting in obtaining electric in accordance with the theoretical values of Donnan equilibrium (Figure 2.7). Under these conditions, the Donnan potential was measured when layering hydrogels with different charges. As a result, it was possible to obtain electric potential profiles corresponding to the internal electric potential changes in the polyelectrolyte hydrogel, demonstrating that this microelectrode technique exhibits sufficient electric potential responsiveness.

Furthermore, Guo et al. elucidated the morphology in the toughness mechanism of DN gels by measuring the electric potential at sites where the DN gel was subjected to tensile damage, comparing it with the electric potential in the bulk, and confirming changes in its internal structure (Figure 2.8) [30]. After sectioning the DN gel into a dumbbell shape, tensile tests were conducted by varying the tensile strain. Subsequently, the electric potential of the swollen and non-swollen zones at each strain in the DN gel was measured after re-swelled. During this process, the measurement focused on the electric potential derived from the first network, which consists of polyelectrolyte network, among the two types of networks composing the DN gel. As a result, the study successfully obtained changes in swelling, measured as variations in electric potential, due to the disruption of the polyelectrolyte network in the DN gel caused by tensile damage. Furthermore, it was discovered that the rupture structure of the first network is larger than the tip diameter of the capillary (approximately 200 nm).

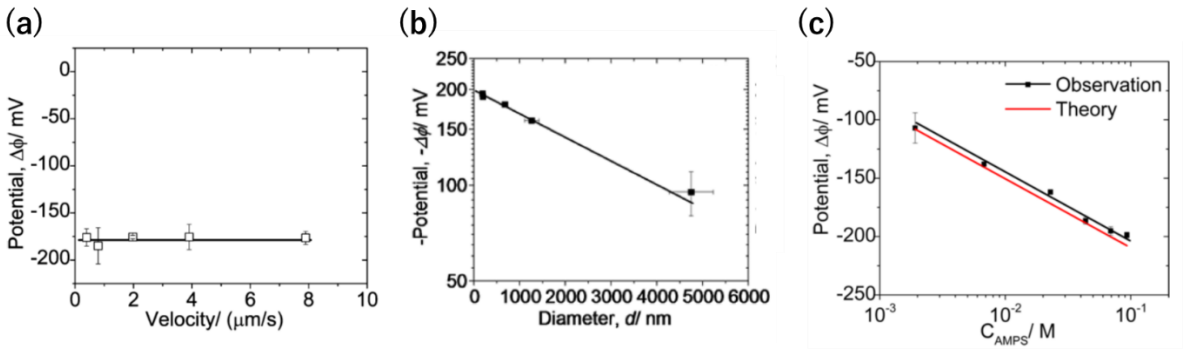

Fig. 2.7 The electric potential of the polyelectrolyte hydrogel when varying the (a) insertion speed and (b) electrode tip diameter, of the capillary. (c) The electric potential profile of the polyelectrolyte hydrogel with varying cross-linking densities measured using a capillary with a tip diameter of 190 nm (Debye length around the capillary is 538 nm). The black line represents the observed electric potential, and the red line represents the theoretical electric potential based on the Donnan equation[30].

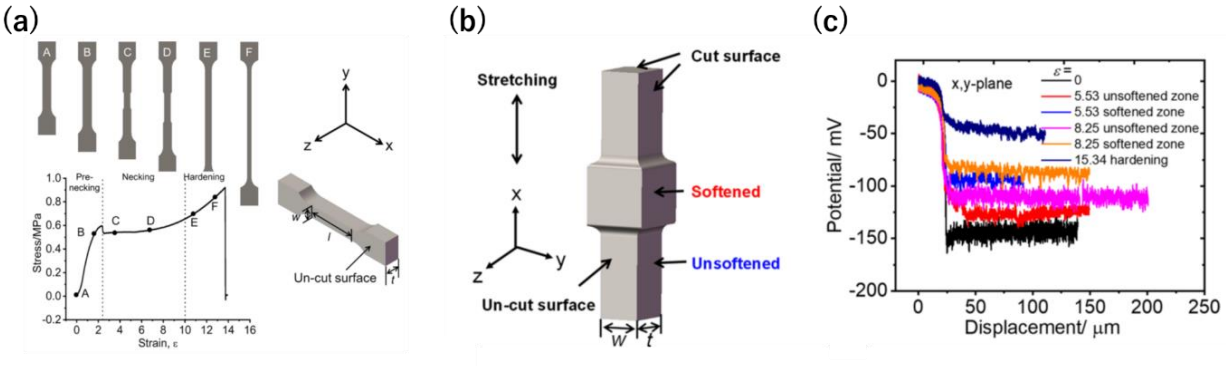

Fig. 2.8 (a) Typical stress-strain curve and schematic illustrations of the specimen at various strains during the uniaxial tensile deformation of a dumbbell-shaped DN gel. (b) Schematic illustration of three different surfaces of a pre-stretched DN gel used to measure the electric potential. (c) Potential profiles of the electric potential measured by the microelectrode technique from the uncut surface (x,y-plane) into the bulk of the DN hydrogel after unloaded from different strains ε[31].

2.4 Objectives of this dissertation

In **Chapter 2,** I introduced background knowledge on polyelectrolyte hydrogels and covered various internal structure analysis methods currently being employed. The heterogeneous internal structure of polyelectrolyte hydrogels and the charge density distribution of electrolyte polymers (polymer concentration distribution) have a significant impact on the mechanical properties and fracture behavior of polyelectrolyte hydrogels. Therefore, evaluating heterogeneity of polyelectrolyte hydrogel spatially and in-situ is important.

In previous studies, the microelectrode technique was demonstrated to be a useful technique for spatially and in-situ measuring the internal structure of polyelectrolyte hydrogels, although providing only average information. On the other hand, when it comes to understanding electric potential changes derived from the heterogeneity in the internal structure of polyelectrolyte hydrogels or the distribution of electrolyte polymer density, the resolution of the microelectrode technique is not sufficient due to issues such as electrical noise and amplifier performance. This inadequacy makes it challenging to distinguish between signal and noise, and prevented a detailed evaluation. Therefore, discussions regarding the internal structure of polyelectrolyte hydrogels using the microelectrode technique have been limited to arguments based on the average values of electric potentials.

Therefore, this dissertation focuses on improving the resolution of the microelectrode technique to establish a technique for spatial and in-situ measurements of the heterogeneous internal structure of polyelectrolyte hydrogels. Specifically, the goal is achieved through the following three steps:

(ⅰ) Improvement of the experimental setup (**Chapter 3**): Enhancing spatial resolution through the replacement of components in the apparatus used for the microelectrode technique and noise reduction.

(ⅱ) Evaluation of the followability of heterogeneous structures (**Chapter 4**): Utilizing the improved microelectrode technique to measure the electric potential of polyelectrolyte hydrogels with known-scale heterogeneous structures and comparing structural sizes.

(ⅲ) Estimation of unknown heterogeneous structures (**Chapters 5 and 6**): Employing the improved microelectrode technique to measure the electric potential of polyelectrolyte hydrogels with unknown-scale internal heterogeneity and making inferences about the internal structure and the distribution of polymer concentrations.

2.5 References

1. 長田義仁, 梶原莞爾, ゲルハンドブック **1997**,エヌ・ティー・エス,
2. Shibayama, M. Spatial inhomogeneity and dynamic fluctuations of polymer gels. *Macromolecular Chemistry and Physics* **1998**, 199 (1).
3. Manning, G. S., Limiting Laws and Counterion Condensation in Polyelectrolyte Solutions .I. Colligative Properties. *J Chem Phys* **1969,** *51* (3), 924-933.
4. Daune, M., Molecular Biophysics: structure in motion. Press, O. U., Ed. *Oxford University Press*: **1999**.
5. Wolfgang Schmickler. Electronic Effects in the Electric Double Layer, *Chem.Rev.* **1996**, 96 (8),3177-3200.
6. D. Eisenberg,; D. Crothers. Physical Chemistry: With Applications to the Life Sciences **1979**.
7. Crothers, D. E. a. D., Physical Chemistry with applications to the life sciences. **1979**; p. p 385.
8. Donnan, F. G. Theorie der Membrangleichgewichte und Membranpotentiale bei Vorhandensein von nicht dialysierenden Elektrolyten. Ein Beitrag zur physikalisch-chemischen Physiologie. *Z. Electrochem* **1911**,17, 572
9. Horkay, F.; Tasaki, I.; Basser, P. J., Osmotic swelling of polyacrylate hydrogels in physiological salt solutions. *Biomacromolecules* **2000,** *1* (1), 84-90.
10. Gong, J. P.; Katsuyama, Y.; Kurokawa, T.; Osada, Y. Double- Network Hydrogels with Extremely High Mechanical Strength. *Adv. Mater.* **2003**, 15, 1155−1158.

11. Yasuda, K.; Gong, J. P.; Katsuyama, Y.; Nakayama, A.; Tanabe, Y.; Kondo, E.; Ueno, M.; Osada, Y. Biomechanical Properties of High-Toughness Double Network Hydrogels. *Biomaterials* **2005**, *26* (21), 4468–4475.

12. Gong, J. P. Why are double network hydrogels so tough? *SoftMatter* **2010**, 6, 2583−2590.

13. Huang, X.; Li, J.; Luo, J.; Gao, Q; Mao, A.; Li, j. Research Progress on Double-network Hydrogels. *Mater. Today Commun.* **2021,** 29, 102757

14. Means ,A. K.; Shrode, C. S.; Whitney, L. V.; Ehrhardt, D. A.;Grunlan, M. A. Double Network Hydrogels That Mimicthe Modulus, Strength, and Lubricity of Cartilage. *Biomacromolecules* **2019**, 20(5), 2034−2042

15. Sun, J. Y.; Zhao, X.; Illeperuma, W. R. K.; Chaudhuri, O.; Oh,K. H.; Mooney, D. J.; Vlassak, J. J.; Suo, Z. Highly stretchable and tough hydrogels. *Nature* **2012**, 489, 133−136.

16. Shibayama, M., Ikkai, F., Shiwa, Y., Rabin, Y. Effect of degree of cross-linking on spatial inhomogeneity in charged gels .1. Theoretical predictions and light scattering study. *Journal of Chemical Physics* **1997**, 107(13) 5227-5235

17. Nakajima, T.; Kurokawa, T.; Ahmed, S.; Wu, W.-L.; Gong, J. P. Characterization of internal fracture process of double network hydrogels under uniaxial elongation. *Soft Matter* **2013**, 9, 1955−1966.

18. Fukao, K.; Nakajima, T.; Nonoyama, T.; Kurokawa, T.; Kawai, T.; Gong, J. P. Effect of relative strength of two networks on the internal fracture process of double network

hydrogels as revealed by in situ small-angle X-ray scattering. *Macromolecules* **2020**, 53, 1154−1163.

19. Cascone, M. G.; Lazzeri, L.; Sparvoli, E.; Scatena, M.; Serino, L. P.; Danti, S. Morphological Evaluation of Bioartificial Hydrogels as Potential Tissue Engineering Scaffolds. *Journal of Materials Science: Materials in Medicine* **2004**, *15* (12), 1309–1313.
20. Kiyama, R,; Yoshida, M,; Nonoyama, T,; Tomas,S,; Jinnai, H,; Kurokawa, T,; Nakajima, T,; Gong, J. P. Nanoscale TEM Imaging of Hydrogel Network Architecture, *Adv.Mater.* **2022**, 2208902-2208902
21. Suzuki, H,; Suzuki, A. AFM observation of polymer gels incorporated with microspheres, *Colloids Surf. A Physicochem.* **1999**, 153, Issues 1–3, 15, 487-493
22. Suzuki, A.; Yamazaki, M.; Kobiki, Y.; Suzuki, H. Surface Domains and Roughness of Polymer Gels Observed by Atomic Force Microscopy. *Macromolecules* **1997**, 30 (8), 2350-2354.
23. L Hodgkin, B. A.; Katz, B.; Biological Association, M. The Effect of Sodium Ions on The Electrical Activity of The Giant Axon of The Squid. *The journal of Physiology* **1949**, 108 (1), 37-77.
24. Lee, C. W.; Szymanska, A. A.; Ikegaya, Y.; Nenadic, Z. The Accuracy and Precision of Signal Source Localization with Tetrodes. In *Proceedings of the Annual International Conference of the IEEE Engineering in Medicine and Biology Society, EMBS*; **2013**; pp 531–534.

25. Takahata, T.; Hayashi, M.; Ishikawa, T. SK4/IK1-like Channels Mediate TEA-Insensitive, Ca 2-Activated K Currents in Bovine Parotid Acinar Cells. *Am J Physiol Cell Physiol* **2003**, *284*, 127–144.

26. Aonuma, H.; Nagayama, T.; Takahata, M. *Distribution of Autofluorescent Cell Bodies in the Crayfish Central Nervous System*; **1996**.

27. Purves, R. D. Microelectrode Methods for Intracellular Recording and Iontophoresis. *Academic Press: London*, **1981**, 33.

28. Rainer W. GüIch, J. H. d., Andrea Weiblea, Thomas Wallmerspergerb, Bernd Kröplinb, Polyelectrolyte gels in electric fields A theoretical and experimental approach. In *In Smart Structures and Materials* **2000***: Electroactive Polymer Actuators and Devices (EAPAD)*, Bar-Cohen, Y., Ed. Proceedings of SPIE: 2000; Vol. 3987.

29. Blyakhman, F. A.; Safronov, A. P.; Zubarev, A. Y.; Shklyar, T. F.; Dinislamova, O. A.; Lopez-Lopez, M. T. Mechanoelectrical Transduction in the Hydrogel-Based Biomimetic Sensors. *Sensors and Actuators, A: Physical* **2016**, *248*, 54–61.

30. Guo, H.; Kurokawa, T.; Takahata, M.; Hong, W.; Katsuyama, Y.; Luo, F.; Ahmed, J.; Nakajima, T.; Nonoyama, T.; Gong, J. P. Quantitative Observation of Electric Potential Distribution of Brittle Polyelectrolyte Hydrogels Using Microelectrode Technique. *Macromolecules* **2016**, *49* (8), 3100–3108.

31. Guo, H.; Hong, W.; Kurokawa, T.; Matsuda, T.; Wu, Z. L.; Nakajima, T.; Takahata, M.; Sun, T.; Rao, P.; Gong, J. P. Internal Damage Evolution in Double-Network Hydrogels Studied by Microelectrode Technique. *Macromolecules* **2019**, *52* (18), 7114–7122.

Chapter 3 Improvement of Microelectrode Technique

3.1 Introduction

In this chapter, I introduce the improved microelectrode technique.

As explained in **Chapter 2**, the microelectrode technique allows for spatial measurements of polyelectrolyte hydrogels. However, in prior research, discussions primarily revolved around the average values of measured Donnan potentials. This was because the resolution of the microelectrode technique was not sufficient for discerning electric potential changes arising from the heterogeneity in the internal structure of polyelectrolyte hydrogels or the distribution of electrolyte polymer density. The issues such as electrical noise and amplifier performance contributed to this lack of resolution.

Therefore, I conducted a thorough reevaluation of both internal and external factors directly influencing the measurement results. Specifically, I aimed to improve spatial resolution by replacing the equipment in the microelectrode electrode system and rigorously blocking noise that could infiltrate from other electronic devices, electromagnetic waves, and power cables. With this improvement, I aimed to measure local electric potential changes within the polyelectrolyte hydrogel with high sensitivity using the improved microelectrode technique, which could previously only be measured using average information. Ultimately, the aim was to represent these variations as a continuous electric potential distribution, enabling a more detailed reflection of the internal heterogeneity within the polyelectrolyte hydrogel.

Additionally, although not directly related to the main focus of this dissertation, I introduce an expansion of the microelectrode technique's apparatus with the expectation of increasing the types of samples that can be measured in the future using this improved technique. Specifically, I demonstrate the construction of a measurement system that can be consistently controlled at any temperature. The microelectrode technique is highly susceptible to external noise, and traditional measurement environments do not control temperature such as heating or cooling. So that, measuring hydrogels at temperatures other than room temperature was challenging in conventional measurement settings.

3.2 Improved the spatial resolution of microelectrode technique

3.2.1 Equipment modification and noise treatment methods

I updated the measurement system to measure the local electric potential of the polyelectrolyte hydrogel more precisely. First, I replaced the oscilloscope with a 12-bit A/D convertor (TELEDYNE LECROY, HDO6034, USA). Next, I performed noise treatment around the wiring. Specifically, ferrite cores (TDK, ZCAT2035-0930A-BK, Japan) were attached to the power cables of each device, and wire mesh shields (MiSUMi, FLS-12-10, Japan) were placed on the outside of the signal cables. I also used a power supply with a ground noise filter (SANWA supply, TAP-3811NFN, Japan). Furthermore, the entire measurement system, excluding the oscilloscope, amplifier, and the manipulator controller, is housed in a custom-made electromagnetic shielding box connected to the ground. The box is covered on all sides with silver-coated conductive electromagnetic shielding mesh. To ensure thorough noise reduction, optimization of cable and device placement was also carried out.

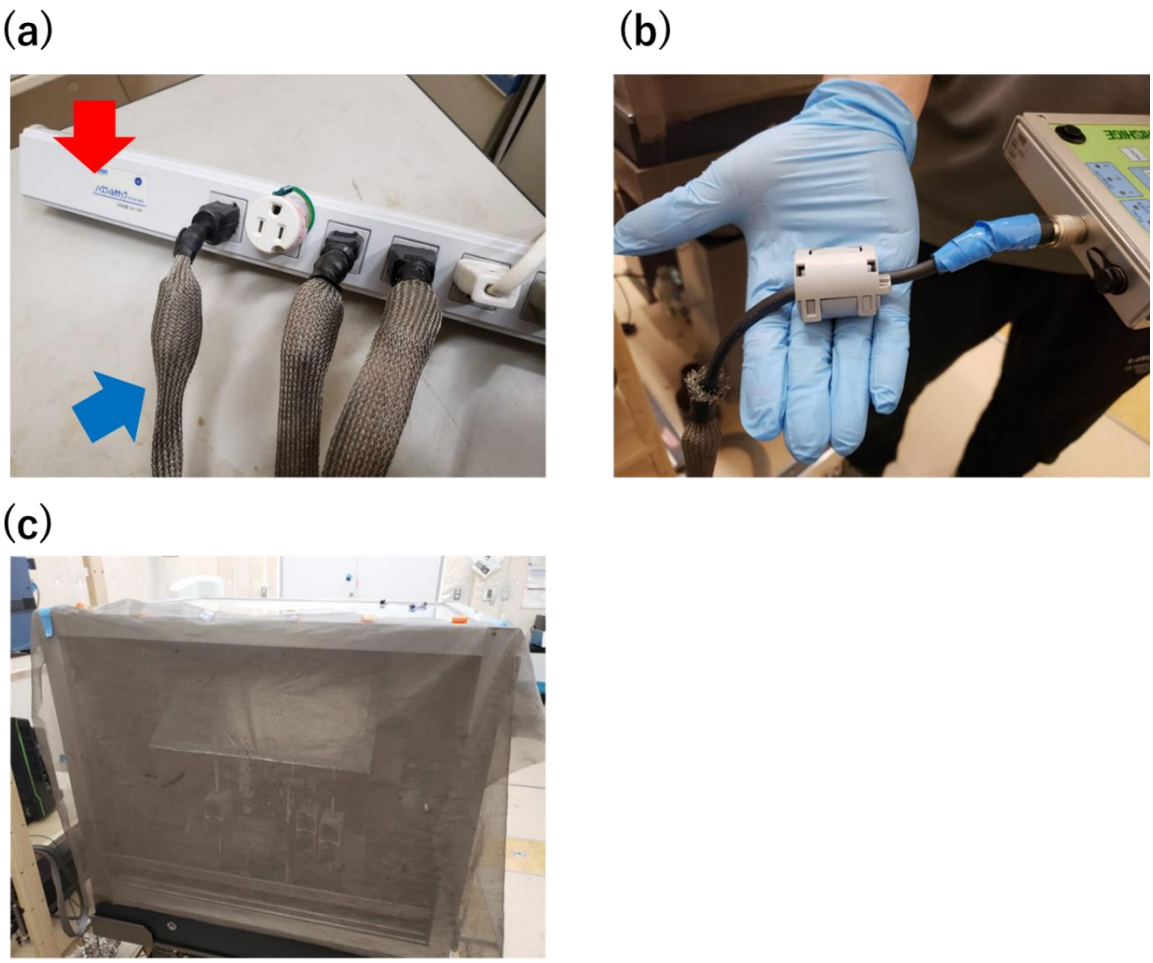

Fig. 3.1 Noise suppression methods. (a) The red arrow indicates a power supply with a ground noise filter, and the blue arrow indicates a wire mesh shield. (b) Ferrite core. (c) Electromagnetic shielding box covered with conductive electromagnetic shielding mesh.

3.2.2 Performance comparison of microelectrode technique before and after modification

The electric potential profile in the reference solution of the previous oscilloscope (Iwatsu, DS-4264, Japan) is shown in Figure 3.2 (a), and the electric potential profile obtained from the new oscilloscope is shown in Figure 3.2 (b). The full scale of the electric potential profile in Figure 3.2(a) measured by the previous oscilloscope was ±1.5 V, the A/D conversion was 8 bits,

the sampling rate was 200 S/s, and the insertion speed of the capillary was 2.0 μm/s. Analysis of these results show that the electric potential resolution of the previous oscilloscope was 6.25 mV, the spatial resolution was 9.9×10^{-3} μm, and the standard deviation of the white noise was ± 3.8 mV. The full scale of the electric potential profile in Figure 3-2 (b) measured by the new oscilloscope was ± 5 V, the A/D conversion was 12 bits, the sampling rate was 2.5 KS /s, and the insertion speed of the capillary was 0.8 μm/s. In contrast to the previous oscilloscope, the new system showed the resolution of the electric potential of the new oscilloscope was 0.1 mV, the spatial resolution was 3.2×10^{-4} μm/S, and the standard deviation of the white noise is ± 0.63 mV. These improvements increased the effective number of samples by a factor of about 38 and allowed us to obtain a spatial resolution of the device sufficient to detect local electric potential changes. Also, I reduced the standard deviation of the white noise to about 1/6. With this reduction, I found that I could detect concentration changes of more than 1.02×10^{-5} M (2%) in a 10^{-5} M $NaCl_{aq}$. It was also assumed that the standard deviation of the white noise does not change regardless of the value of the electric potential[1].

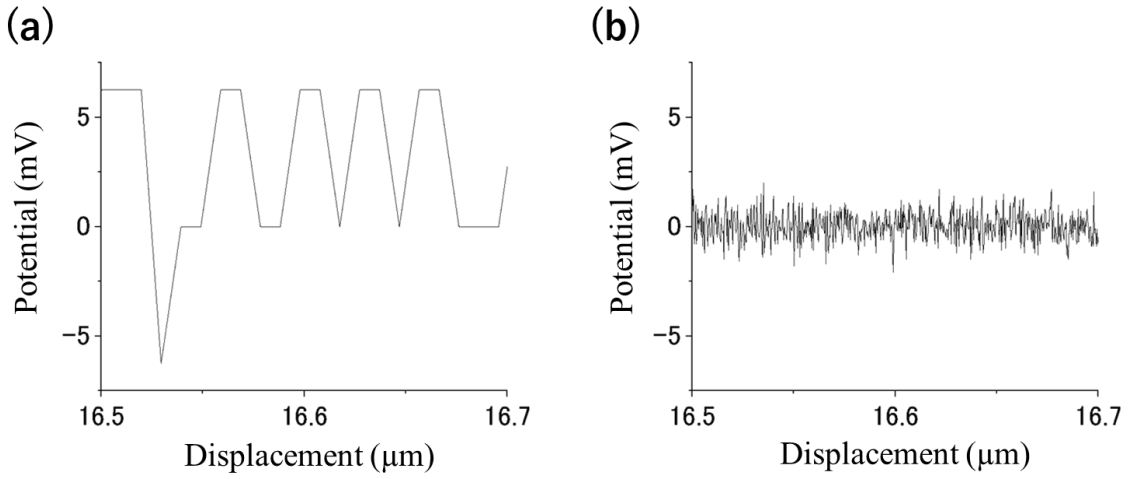

Fig.3.2 The electric potential fluctuation and noise in 10^{-5} M $NaCl_{aq}$ solution reported in a previous study compared to the results obtained in the current work[3]. (a) The profile obtained by the previous method with an older oscilloscope: the electric potential resolution was 6.25 mV, and the spatial resolution was 9.9×10^{-3} μm. (Conditions: electric potential full scale, ±1.5 V; A/D conversion, 8 bit; sampling rate, 200 /s; insert speed, 2.0 μm/s). (b) The profile obtained in this work with the new oscilloscope: the electric potential resolution is 0.1 mV, and the spatial resolution is 3.2×10^{-4} μm. (Conditions: electric potential full scale, ±5 V; A/D conversion, 12 bit; sampling rate, 2500 /s; insert speed, 0.8 μm/s).

3.3 Expansion the temperature control system of microelectrode technique

3.3.1 Strategy for construction of insulation system

In constructing the insulation system, it is crucial not only to maintain a constant temperature but also to ensure that noise from the insulation system does not affect the electric potential measurements. Initially, I had considered designing an insulation system using peltier elements. However, electric noise was significantly high, causing the polyelectrolyte hydrogel's electric potential to be obscured by the noise. Therefore, I created an insulation system using a water recirculation device, as shown in Figure 3-3 (a). The main body of the water recirculation device can be placed away from the Donnan measurement apparatus, and it has the advantage of being less prone to becoming a source of noise since it simply draws cold and hot water into the measurement system using hoses. Next, I created a container with a water flow path using polycarbonate, a highly insulating material, as shown in Figure 3-3 (b). The design ensures that the temperature of the entire container remains constant. I then placed an aluminum plate with good thermal conductivity on the lid portion of the container and set a glass container on top for placing the hydrogel. Holes were provided in the lid portion of the glass container for passing two electrodes.

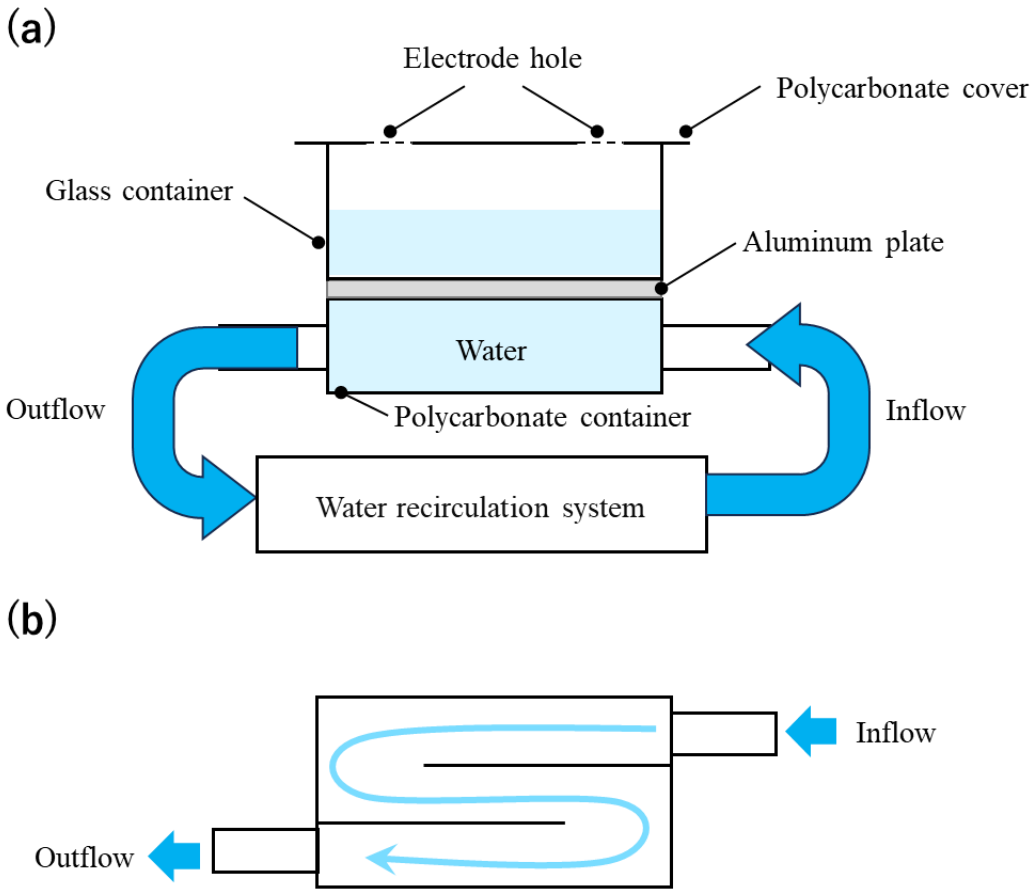

Fig. 3.3 (a) Diagram of the insulation system using a water recirculation device. By recirculating cold and hot water within the polycarbonate container using the water recirculation device, it is possible to maintain a constant temperature inside the glass container. To prevent temperature changes due to evaporation, a polycarbonate lid is used, and two small holes are provided in the lid for passing electrodes. (b) Top view of the polycarbonate container. A water flow path is designed to ensure that temperature variations do not occur within the container.

3.3.2 Performance evaluation of the insulation system

To verify the performance of the insulation system, I set the recirculation device temperature to 40℃ and placed a 10-5 M NaCl solution inside the glass container. The temperature variation was then measured using a Thermometer (TR-71U, T and D, Japan), and the results are shown in Figure 3.4 (a). As a result, it was observed that despite a slight difference of 1-2℃ between the recirculation device and the glass container, the temperature of the solution inside the glass container remained relatively constant. This slight temperature decrease may be attributed to the passage of the hose. Furthermore, the electric potential when inserting it into the 10^{-5} M $NaCl_{aq}$ inside the glass container, with a sampling rate of 2.5 MS/s and a capillary insertion speed of 2.0 μm/s, is shown in Figure 3.4 (b). The standard deviation of the white noise at this time was ±0.86 mV. Considering that the standard deviation of the electric potential before attaching the recirculation device was ±0.63 mV, although the noise slightly increased, it was found to have minor impact on the measurement, and effective electric potential data could be obtained.

Based on the above, the creation of an insulation system for the microelectrode technique's system has been successful. With this insulation system, it is anticipated that the microelectrode technique can be applied to various samples, such as functionally graded hydrogels which undergo phase separation at different temperatures, or equipment for cell culture, enabling measurements under controlled temperature conditions.

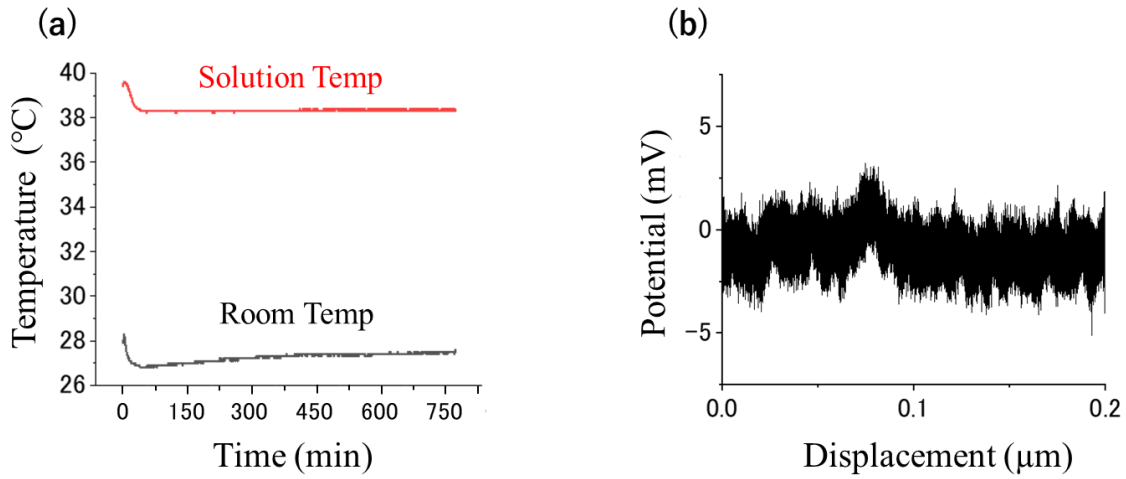

Fig. 3.4 (a) Temperature changes in the 10^{-5} M $NaCl_{aq}$ inside the glass container measured using a thermometer. The recirculation device was set to 40°C, and the ambient temperature was 27°C. The red line represents the temperature of the solution, and the black line represents the room temperature. (b) Potential profile when the electrode was inserted into the 10^{-5} M $NaCl_{aq}$ inside the glass container. (Conditions: electric potential full scale, ±5 V; A/D conversion, 12 bit; sampling rate, 2.5 MS/s; insert speed, 2.0 μm/s).

3.4 References

1. Guo, H.; Kurokawa, T.; Takahata, M.; Hong, W.; Katsuyama, Y.; Luo, F.; Ahmed, J.; Nakajima, T.; Nonoyama, T.; Gong, J. P. Quantitative Observation of Electric Potential Distribution of Brittle Polyelectrolyte Hydrogels Using Microelectrode Technique. *Macromolecules* **2016**, *49* (8), 3100–3108.
2. Guo, H.; Hong, W.; Kurokawa, T.; Matsuda, T.; Wu, Z. L.; Nakajima, T.; Takahata, M.; Sun, T.; Rao, P.; Gong, J. P. Internal Damage Evolution in Double-Network Hydrogels Studied by Microelectrode Technique. *Macromolecules* **2019**, *52* (18), 7114–7122.
3. Nishimura, T.; Guo, H.; Kiyama, R.; Katsuyama, Y.; Gong, J.P.; Kurokawa, T. In Situ Evaluation of the Polymer Concentration Distribution of Microphase-Separated Polyelectrolyte Hydrogels by the Microelectrode Technique. *Macromolecules* **2021**, 54, 10776–10785.

Chapter 4 Spatial distribution measurement of μm scale heterogeneous structures by microelectrode technique

4.1 Introduction

In order to employ the improved microelectrode technique for measuring the heterogeneous internal structure of a polyelectrolyte hydrogel, it is essential to determine the extent to which it can measure the heterogeneous structure in terms of scale. Therefore, in this chapter, I first polymerized a polyelectrolyte hydrogel with a known μm-scale heterogeneous structure. Subsequently, I attempted to measure the electric potential and evaluate the internal structure using this gel.

As a model material with μm-scale heterogeneous structures, I employed a particle DN Gel (P-DN Gel)[1-3]. This gel incorporates polyelectrolyte micro-particle hydrogels, with diameters on the order of tens of micrometers, into a neutral hydrogel (non-polyelectrolyte hydrogel). Micro-particle hydrogels are defined by IUPAC[4] as "gel particles of any shape with diameters ranging from approximately 0.1 to 100 μm."

While P-DN Gel lacks the toughness and strength of DN Gel[5,6], it exhibits higher formability in comparison. The reason for the higher formability of P-DN gel lies in the fact that the first network assumes a particulate form, and during the polymerization stage of P-DN gel, the polyelectrolyte micro-particle hydrogels reach equilibrium swelling. Consequently, after polymerization, the P-DN gel undergoes minimal additional swelling until it reaches equilibrium swelling again. This property allows it to retain the shape of the mold during creation. Therefore, P-DN gel is expected to find applications as biomimetic materials, such as

in artificial menisci (e.g., artificial half-meniscus)[1]. Additionally, it is already being utilized industrially as a filler for gel 3D printers[7]. On the other hand, due to the distribution of polyelectrolyte micro-particle hydrogels in three-dimensional space, understanding the fracture behavior and mechanical properties of P-DN gel accurately can be challenging. To comprehend these aspects, it is essential to have knowledge of the internal distribution of micro-particle hydrogels.

Therefore, in this chapter, I employed the improved microelectrode technique to measure the electric potential of P-DN gel. By comparing the size of polyelectrolyte micro-particle hydrogels with the structural size obtained from electric potential measurements, I verified the followability of the microelectrode technique in measuring the heterogeneous internal structure of polyelectrolyte hydrogels. Furthermore, through 3D color mapping of spatially distributed polyelectrolyte micro-particle hydrogels, I visualized the μm-scale heterogeneous internal structure and confirmed the feasibility of measuring the spatial distribution of polyelectrolyte micro-particle hydrogels.

4.2 Experimental section

4.2.1 Materials

2-Acrylamido-2-methylpropanesulfonic acid sodium salt (NaAMPS) was provided as a courtesy from Toagosei Co. Ltd, Japan. Dimethylacrylamide (DMAAm), N,N′-Methylenebis(acrylamide) (MBAA), 2-oxoglutaric acid (OA), sodium chloride (NaCl), and kerosene were purchased from Wako Pure Chemical Industries, Ltd. SY-Glyster CR-310 was purchased from Sakamoto Yakuhin Kogyo Co., Ltd. All these materials were used as received.

4.2.2 Synthesis of polyelectrolyte micro-particle hydrogels

I prepared polyelectrolyte micro-particle hydrogels. Negatively charged monomer (NaAMPS: 1 M), cross-linker (MBAA: 4 mol% relative to NaAMPS concentration), and initiator (OA: 0.1 mol% relative to NaAMPS concentration) were dissolved in pure water. This solution was emulsified for 2 hours in a mixed solution of kerosene and surfactant using the SPG (Spinning Particle Gelation) membrane emulsification method, resulting in particle formation. At this time, the pore size of the SPG membrane used was 5 μm, the surfactant employed was SY-Glyster CR-310, the gas pressure was 10 kPa, and the stirring speed was set at 400 rpm. Then, the solution was irradiated with UV light (365 nm; 4 mW/cm^2) for 8 hours under an argon atmosphere. After polymerization, the polyelectrolyte micro-particle hydrogels were immersed in an isopropyl solution to remove the surfactant.

4.2.3 Synthesis of P-DN gels

After freeze-drying the synthesized polyelectrolyte micro-particle hydrogels, they were mixed with a gel precursor solution containing neutral monomers at a ratio of 12 g of polyelectrolyte micro-particle hydrogels per 100 ml of the solution. The gel precursor solution

was made from neutral monomer (DMAAm: 2 M), cross-linker (MBAA: 0.02 mol% relative to DMAAm concentration), and initiator (OA: 0.01 mol% relative to DMAAm concentration). After letting the mixed solution stand for one day, the supernatant layer containing only the DMAAm solution was removed. The mixed solution was poured into a glass mold consisting of two soda-lime glass plates (thickness = 3 mm), separated by a O-shaped silicone rubber sheet (thickness = 2 mm). The mold was irradiated with UV light (365 nm; 285 mW/cm^2) for 30 minutes under air. After letting the synthesized P-DN Gel sit in a darkroom for one day, it was subsequently immersed in deionized water. To thoroughly remove any remaining monomers or initiators, the immersed pure water was exchanged daily for approximately one month. After completing the removal of monomers, the P-DN gel was immersed in a 10-5 M $NaCl_{aq}$ for two days to achieve an equilibrium state.

4.2.4 Electric potential measurement of P-DN gels[8-10]

The P-DN gel with completed solvent replacement is impregnated into a fresh 10^{-5} M $NaCl_{aq}$ container. The container was fixed on an XY stage (LD-6042-C7, Chuo Seiki) so that it could be moved in 1 μm increments in the direction of crack propagation. The capillaries were made by stretching a glass tube (BF100-75-15, Sutter, USA) using a Puller (P-2000, Sutter, USA). The diameter of the glass tube was 0.78 mm, and the total length was about 7.5 cm. The tip length and diameter of the capillaries varied depending on various parameters such as stretching speed, stretching force, and stretching time. The electrical resistance in the reference solution also varies with these parameters. In this system, capillaries with a tip diameter of about 150 nm, a resistance value of 20-60 MΩ, and a vertically aligned diameter were prepared. A capillary controlled by a micromanipulator (DMA-1511, Narishige, Japan) was inserted into the P-DN gel from an external reference solution at 0.8 μm/sec. Furthermore, to measure 3D

color mapping, electric potential measurements were taken at 48 locations on a portion of the P-DN gel surface (area: 50 μm × 70 μm) at intervals of 10 μm.

4.3 Result and Discussion

4.3.1 The electric potential profile of the P-DN gel

The results of measuring the electric potential of the P-DN Gel are shown in Figure 4.1. A binary electric potential profile resembling a rectangular wave with two electric potential ranges, -40 mV and -170 mV, was obtained. It is inferred that the electric potential range of -170 mV corresponds to the polyelectrolyte micro-particle hydrogels, while the electric potential range of -40 mV corresponds to the bulk neutral hydrogel. Here, while the bulk hydrogel is composed of a neutral polymer without a charge, it is considered that residual polyelectrolyte monomers within the polyelectrolyte micro-particle hydrogels undergo partial copolymerization with neutral monomers during the P-DN gel polymerization[11]. Therefore, the electric potential of the bulk hydrogel is not expected to be a complete 0 mV. Based on the above results, it is evident that the microelectrode technique allows for the measurement of the polyelectrolyte micro-particle hydrogels within the P-DN gel.

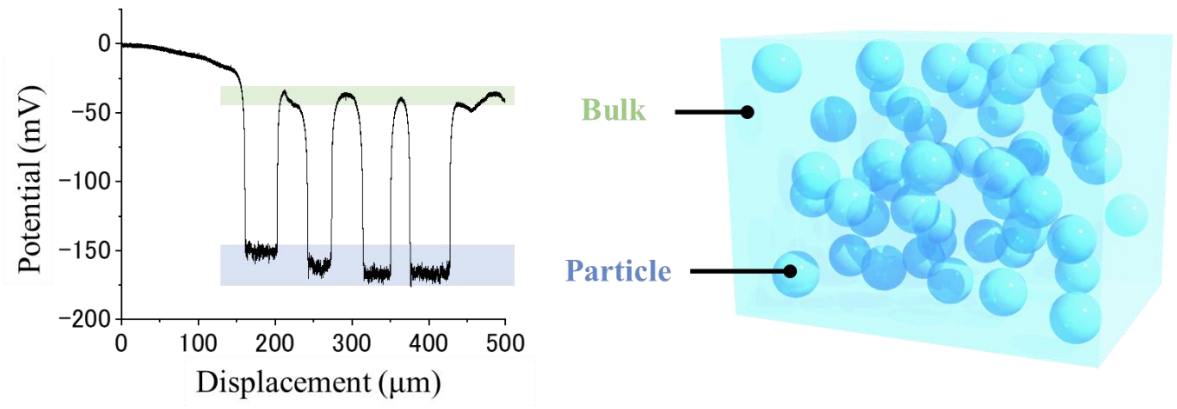

Fig. 4.1 The electric potential profile of the P-DN gel. It exhibited a binary electric potential profile, with two electric potential ranges: -170 mV representing the polyelectrolyte micro-particle hydrogels and -40 mV representing the neutral bulk hydrogel.

4.3.2 Verification of structure size measured by microelectrode technique

Figure 4.2 (a) shows the results of observing the P-DN gel under a microscope (Eclipse LV100N POL, Nikon Co., Japan). From the obtained microscopic images, the diameter (ξ_{op}) of the polyelectrolyte micro-particle hydrogels were measured using ImageJ, and it was found to be approximately 55 μm. On the other hand, Figure 4.2 (b) represents an enlarged view of the electric potential range of the polyelectrolyte micro-particle hydrogels obtained through the microelectrode technique. The structure size of polyelectrolyte micro-particle hydrogels (ξ_{MET}) that can be measured using the microelectrode technique is determined by the displacement of the capillary within the polyelectrolyte micro-particle hydrogels. It was found to be approximately 40 μm. This is likely due to the small diameter of the capillary relative to the polyelectrolyte micro-particle hydrogels, as illustrated in Figure 4.3(a). While the diameter can always be measured in microscopic images, the microelectrode technique measurement is influenced by variations in the measured structure size of the polyelectrolyte micro-particle hydrogels depending on the location where the capillary is inserted.

Therefore, I investigated the validity of the structure size of the polyelectrolyte micro-particle hydrogels measured by the microelectrode technique in comparison to the actual size of them. The assumption is made that the polyelectrolyte micro-particle hydrogels are a true sphere. Given that the size of polyelectrolyte micro-particle hydrogels is significantly larger than the tip diameter of the capillary, let's consider a plane that includes the sphere center and the insertion position of the capillary, as illustrated in Figure 4.3 (b).

Assuming the center of the polyelectrolyte micro-particle hydrogel as the origin, the diameter of the inserted polyelectrolyte micro-particle hydrogels as $2r$, and the average

distance inserted by the capillary within the polyelectrolyte micro-particle hydrogels as $2\bar{r}$, with $\bar{r} = rsin\theta$ for $0 \leqq \theta \leqq \pi$ as θ.

Then, the expression for $\bar{r}$ in relation to a circle with radius r is given as follows:

$$\bar{r} = \frac{1}{2r}\int_{-r}^{r} y\,dx \qquad (x:\ r \to -r,\ y: 0 \to r \to 0\ ) \quad (4.1)$$

Here, since $y = rsin\theta, x = rcos\theta$ $(\theta: \pi \to 0)$, the following relationship between $\bar{r}$ and r is obtained:

$$\bar{r} = \frac{1}{2r}\int_{-r}^{r} y\,dx = \frac{1}{2r}\int_{\pi}^{0} rsin\theta\left(\frac{d\ \mathrm{rcos}\ \theta}{d\ \theta}\right) = \frac{r}{4}\pi \quad (4.2)$$

Given that the size of the polyelectrolyte micro-particle hydrogel measured by the microscope is $2r$, if I set $2r = 55$, it can calculate $2\bar{r}$ as follows:

$$2r : 2\bar{r} = 1 : \frac{\pi}{4} = 55 : 2\bar{r} \ \rightleftarrows\ 2\bar{r} = 43.2 \quad (4.3)$$

From this, the theoretical value of the average structural size obtained when a capillary is randomly inserted into the polyelectrolyte micro-particle hydrogels is approximately 43 μm. This ideal size is consistent with the structure size of the polyelectrolyte micro-particle hydrogels obtained by microelectrode technique.

Based on the above discussion, the size of the polyelectrolyte micro-particle hydrogels measurable by the microelectrode technique was found to be consistent with the actual size of the polyelectrolyte micro-particle hydrogels. Therefore, it was confirmed that the internal

structure of polyelectrolyte hydrogels with μm-scale heterogeneous structures can be measured with high sensitivity using the microelectrode technique.

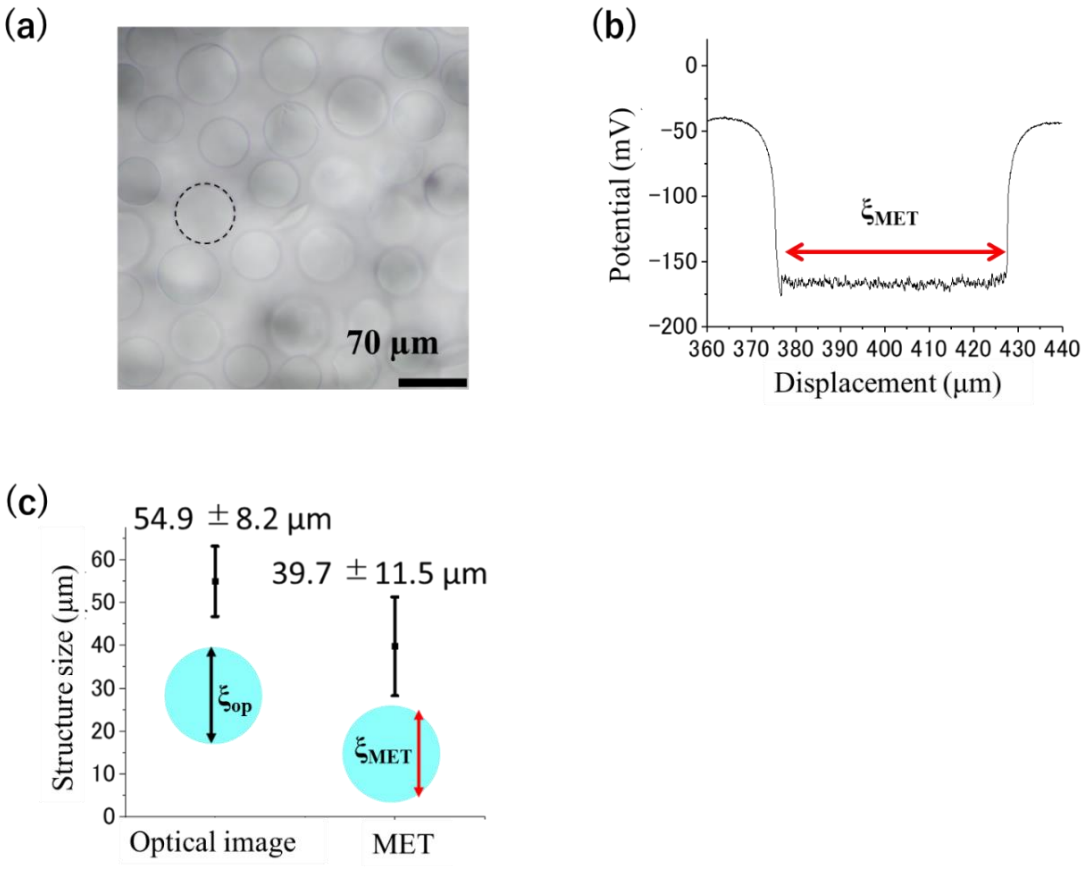

Fig. 4.2 (a) Microscopic image of P-DN gel. (b) Enlarged view of the polyelectrolyte micro-particle hydrogels in the electric potential profile of P-DN gel. ξ_{MET} represents the structural size measurable by the microelectrode technique, indicating the distance inserted by the capillary through the polyelectrolyte micro-particle hydrogels. (c) Average structural size by calculated by microscopic images and electric potential profiles. ξ_{op} represents the diameter of t the polyelectrolyte micro-particle hydrogels.

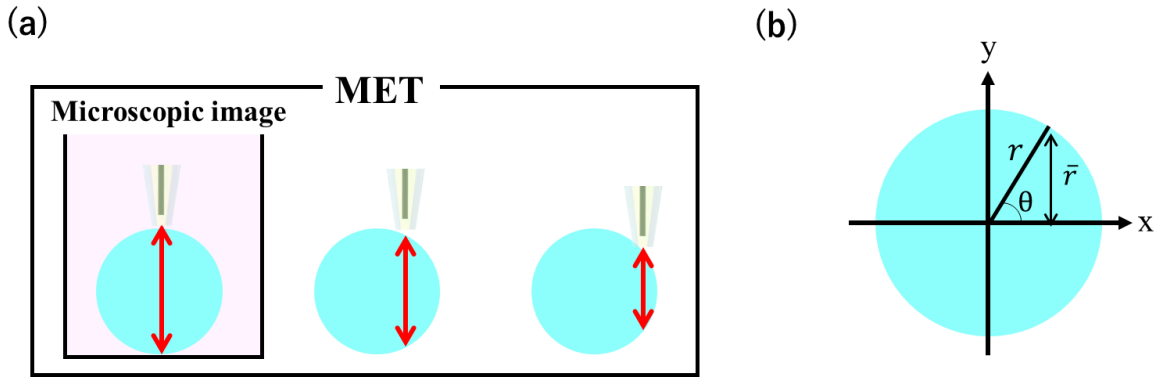

Fig. 4.3 (a) The structure size measurable by the microelectrode technique and microscopy. (b)A planar diagram with the center of the sphere as the origin and the point where the capillary is inserted. the diameter of the inserted polyelectrolyte micro-particle hydrogels as $2r$, and the average distance inserted by the capillary within the polyelectrolyte micro-particle hydrogels as $2\bar{r}$, with $\bar{r} = rsin\theta$ for $0 \leqq \theta \leqq \pi$ as θ.

4.3.3 3D color mapping of polyelectrolyte micro-particle hydrogels inside the P-DN gel

The use of the microelectrode technique has successfully measured the internal structure of the P-DN gel, but the obtained electric potential profile is limited to the depth direction of the P-DN gel. Therefore, as shown in Figure 4.4 (a), I measured electric potential at 48 locations on a portion of the P-DN gel surface (area: 50 μm × 70 μm) at intervals of 10 μm. Next, I classified the electric potential range of polyelectrolyte micro-particle hydrogel at each position into 8-gradeations in a range of -125 mV to -195 mV with a 10 mV interval, as illustrated in Figure 4.4 (b). By considering the P-DN gel surface as Depth 0 μm and arranging the color profiles classified into 8-gradeations at each position, I created 3D color mapping, resulting in Figure 4.4 (c).

I was able to observe structures resembling hemispheres and continuous arrangements of spheres through 3D color mapping. The diameter of polyelectrolyte micro-particle hydrogels used in this experiment is approximately 55 μm. Therefore, within the measurement range, it was not possible to completely observe one polyelectrolyte micro-particle hydrogel, but successful visualization of the spatial distribution of polyelectrolyte micro-particle hydrogels within the P-DN gel was achieved. These results indicate that the microelectrode technique is capable of spatially measuring μm-scale heterogeneous structures of polyelectrolyte hydrogel.

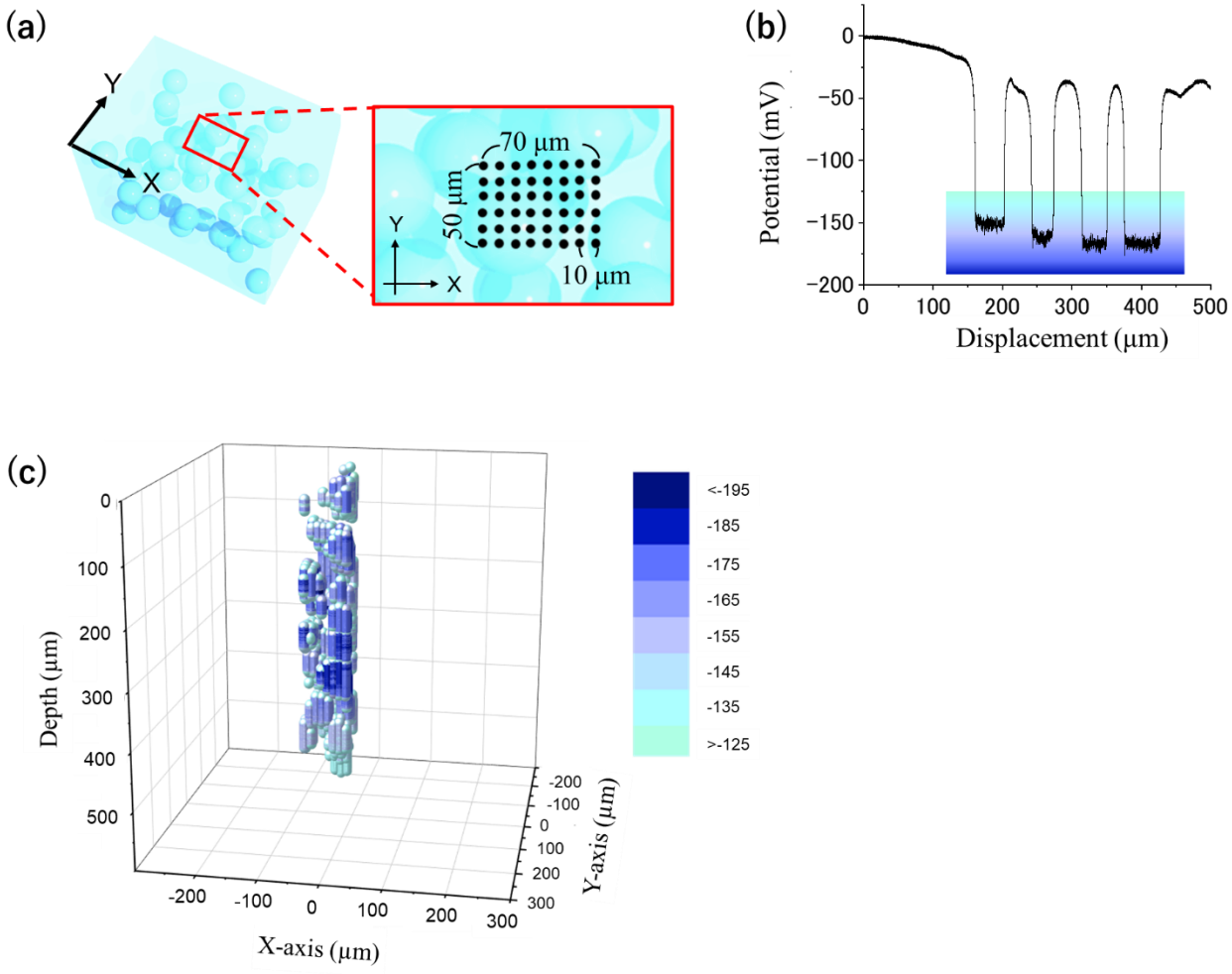

Fig. 4.4 (a) Schematic diagram representing the points where electric potential measurements were conducted for 3D color mapping. (b) Tonal classification of the electric potential profile. It classified 8-gradeations in a range of -125 mV to -195 mV with a 10 mV interval. (c) 3D color mapping of P-DN gel.

4.4 Conclusion

In this chapter, P-DN gel, which encapsulates polyelectrolyte micro-particle hydrogels within a neutral gel, was created, and its electric potential was measured using the improved microelectrode technique. As a result, a rectangular wave-like electric potential profile, alternating between the electric potential range representing bulk hydrogel and that representing polyelectrolyte micro-particle hydrogels, was obtained. The size of the polyelectrolyte micro-particle hydrogels obtained through the microelectrode technique were found to be valid when compared to those obtained from microscopy. Therefore, it was confirmed that the microelectrode technique can measure the internal structure of P-DN gel. Furthermore, by comprehensively measuring the electric potential over a certain range in the P-DN gel and performing 3D color mapping, it was possible to visualize the polyelectrolyte micro-particle hydrogel inside P-DN gel, which was difficult with conventional structural measurement methods. From the above, it has become evident that the improved microelectrode technique is capable of spatially measuring μm-scale heterogeneous structures of polyelectrolyte hydrogels.

4.5 References

1. Saito, J.; Furukawa, H.; Kurokawa, T.; Kuwabara, R.; Kuroda, S.; Hu, J.; Tanaka, Y.; Gong, J. P.; Kitamura, N.; Yasuda, K. Robust bonding and one-step facile synthesis of tough hydrogels with desirable shape by virtue of the double network structure. *Polym. Chem.* **2011**, 2, 575.
2. Hu, J.; Hiwatashi, K.; Kurokawa, T.; Liang, S. M.; Wu, Z. L.; Gong, J. P. Microgel-Reinforced Hydrogel Films with High Mechanical Strength and Their Visible Mesoscale Fracture Structure. *Macromolecules* **2011**, 44, 7775.
3. Hu, J.; Kurokawa, T.; Hiwatashi, K.; Nakajima, T.; Wu, Z. L.; Liang, S. M.; Gong, J. P. Structure Optimization and Mechanical Model for Microgel-Reinforced Hydrogels with High Strength and Toughness. *Macromolecules* **2012**, 45, 5218-5228.
4. Aleman, J.; Chadwick, A. V.; He, J.; Hess, M.; Horie, K.; Jones, R. G.; Kratochvil, P.; Meisel, I.; Mita, I.; Moad, G.; Penczek, S.; Stepto, R. F. T. *Pure Appl. Chem.* **2007**, 79, 1801.
5. Gong, J. P.; Katsuyama, Y.; Kurokawa, T.; Osada, Y. Double- Network Hydrogels with Extremely High Mechanical Strength. *Adv. Mater.* **2003**, 15, 1155−1158.
6. Yasuda, K.; Gong, J. P.; Katsuyama, Y.; Nakayama, A.; Tanabe, Y.; Kondo, E.; Ueno, M.; Osada, Y. Biomechanical Properties of High-Toughness Double Network Hydrogels. *Biomaterials* **2005**, 26 (21), 4468–4475.
7. R. Hidema ,; K. Sugita, ; H. Furukwa. 3-Dimensional Freeform Fabrication of High-Strength Gels by Laser Scanning Irradiation *Trans. J. Soc. Mech. Eng. (A)* **2011**, 77, 1002-1006
8. Nishimura, T.; Guo, H.; Kiyama, R.; Katsuyama, Y.; Gong, J.P.; Kurokawa, T. In Situ Evaluation of the Polymer Concentration Distribution of Microphase-Separated Polyelectrolyte Hydrogels by the Microelectrode Technique. *Macromolecules* **2021**, 54, 10776–10785.

9. Guo, H.; Kurokawa, T.; Takahata, M.; Hong, W.; Katsuyama, Y.; Luo, F.; Ahmed, J.; Nakajima, T.; Nonoyama, T.; Gong, J. P. Quantitative Observation of Electric Potential Distribution of Brittle Polyelectrolyte Hydrogels Using Microelectrode Technique. *Macromolecules* **2016**, *49* (8), 3100–3108.
10. Guo, H.; Hong, W.; Kurokawa, T.; Matsuda, T.; Wu, Z. L.; Nakajima, T.; Takahata, M.; Sun, T.; Rao, P.; Gong, J. P. Internal Damage Evolution in Double-Network Hydrogels Studied by Microelectrode Technique. *Macromolecules* **2019**, *52* (18), 7114–7122.
11. Frauenlob, M.; Guo, H.; Kurokawa, T.; Gong, J. P. Origin of Surface Charge of Double Network Hydrogels Prepared by Sequential Polymerization. *Macro Letters* **2023**, 12,860-865

Chapter 5 In-situ evaluation of the polymer concentration distribution of microphase separated polyelectrolyte hydrogels by microelectrode technique

This work was reprinted with permission from " Nishimura, T.; Guo, H.; Kiyama, R.; Katsuyama, Y.; Gong, J.P.; Kurokawa, T. In Situ Evaluation of the Polymer Concentration Distribution of Microphase-Separated Polyelectrolyte Hydrogels by the Microelectrode Technique. *Macromolecules* **2021**, 54, 10776–10785. Copyright 2024 American Chemical Society." This chapter has been modified from its original form.

5.1 Introduction

In **Chapter 4**, it was demonstrated that the improved microelectrode technique can measure the μm-scale heterogeneous structure of polyelectrolyte hydrogels. In this chapter, the microelectrode technique was employed for electric potential measurements to infer the structure of polyelectrolyte hydrogels with unknown-scale heterogeneous internal structures. The goal was to confirm the utility of the microelectrode technique as a measurement technique for the internal structure of heterogeneous polyelectrolyte hydrogels and to explore the limitations of the scale of heterogeneity that can be measured using this technique.

As a hydrogel model with unknown-scale heterogeneity, a hydrogel with an internal structure where polyelectrolyte network undergoes phase separation into sea-island structures, hereafter referred to as a phase separated gel, is used[1]. The phase separated gel was synthesized

by using a dioxane/water mixed solvent in the precursor monomer solution of the gel. Since dioxane is a poor solvent for the polymer, it is possible to create a polyelectrolyte hydrogel with a non-uniform phase separated structure consisting of a dense phase and a sparse phase. We can adjust the degree of internal phase separation of this gel by varying the fraction of dioxane in the mixture solvent.

Therefore, I used the improved microelectrode technique[2] to measure the electric potential of phase separated gels with different degrees of internal phase separation, and I estimated the internal structure of phase separation. And based on the electric potential measurement results, I derived the polymer concentration distribution and quantitatively calculated the polymer concentrations in the dense and sparse phases of the phase-separated system. Moreover, I estimated the spatial resolution of microelectrode technique from the aggregate sizes obtained in the electric potential profile and verified the validity of the aggregate sizes through comparison with TEM images.

5.2 Experimental section

5.2.1 Materials

2-Acrylamido-2-methylpropanesulfonic acid sodium salt (NaAMPS) was provided courtesy of Toa Gosei Co., Ltd. Dimethylacrylamide (DMAAm), N, N′-Methylenebis(acrylamide) (MBAA), 2-oxoglutaric acid (OA), potassium chloride (KCl), sodium chloride (NaCl), iron (Ⅲ) chloride hexahydrate, iron (Ⅱ) chloride tetrahydrate and 1,4-dioxane were purchased from FUJIFILM Wako Pure Chemical Industries, Ltd. All materials were used as received.

5.2.2 Synthesis of phase separated single network gels[1]

I prepared hydrogels with dioxane, resulting in an internally phase separated structure. Dioxane is a poor solvent for poly(NaAMPS) while NaAMPS monomers are soluble in dioxane. Therefore, when the monomer is dissolved in a mixture of dioxane and water and polymerized, the polymer aggregates during polymerization. Negatively charged monomer (NaAMPS: 1 M), cross-linker (MBAA : 3 mol% relative to NaAMPS concentration), and initiator (OA: 0.1 mol% relatives to NaAMPS concentration) were dissolved in a mixed solvent. The dioxane weight fractions (r) of mixed solvents were 0, 0.1, 0.2, 0.3, 0.4, 0.5, and 0.54. I poured the solution into a glass mold consisting of two soda-lime glass plates (thickness = 3 mm) separated by a U-shaped silicone rubber sheet (thickness = 2 mm). The mold was irradiated with UV light (365 nm; 4 mW / cm^2) for 9 hours. The prepared hydrogels were immersed in deionized water, and the immersion water was changed daily for about two weeks to remove dioxane, residual monomers, and initiators. The degree of removal of residual monomers and other substances

was checked using a conductivity meter. Gas chromatography (GC-2014, SHIMADZU, Japan) was used to check the residual dioxane concentration in the washing solution.

5.2.3 Synthesis of phase separated DN gels[3,4]

The phase separated single network gels after the removal of residues were very brittle and unsuitable for microelectrode technique. Therefore, I increased the toughness of the phase separated gel by employing the double network concept. Neutral monomers were used as the reinforcing network as to not affect the microelectrode technique. The phase separated gels were immersed in an aqueous solution of a neutral monomer (DMAAm: 2 M), cross-linker (MBAA: 0.1 mol% of DMAAm concentration), and initiator (OA: 0.1 mol% of DMAAm concentration) for two days. After immersion, the poly(NaAMPS) gel was sandwiched between two soda-lime glass plates. The gels were then irradiated with UV light (365 nm; 4 mW/cm^2) for 9 h under Ar atmosphere. The prepared hydrogels were immersed in deionized water, and the soaking water was changed daily for about one month to remove residual monomer and initiator. After that, the phase separated DN gel swollen to 3-5 mm in thickness was immersed in 10^{-5} M $NaCl_{aq}$ for more than two days to reach equilibrium.

5.2.4 Electric potential measurement of the phase separated DN gels[2,5,6]

The capillaries were made by stretching a glass tube (BF100-75-15, Sutter, USA) using a Puller (P-2000, Sutter, USA). The diameter of the glass tube was 0.78 mm, and the total length was about 7.5 cm. The tip length and diameter of the capillaries varied depending on various parameters such as stretching speed, stretching force, and stretching time. The electrical resistance in the reference solution also varies with these parameters. In this system, capillaries with a tip diameter of about 150 nm, a resistance value of 20-60 MΩ, and a vertically aligned

diameter were prepared. A capillary controlled by a micromanipulator (DMA-1511, Narishige, Japan) was inserted into the phase separated DN gel from an external reference solution at 2 μm/sec. The reference solution was 10^{-5} M $NaCl_{aq}$.

5.2.5 Imaging of phase separated DN gels by TEM[7]

To stain the polyelectrolyte, I mineralized Fe particles in the poly(NaAMPS) network of a phase separated DN gel. The staining solutions used were 2.5 M $FeCl_3$ and 1.5 M $FeCl_2$. Amorphous iron oxide nanoparticles were grown on the poly(NaAMPS) network by immersing the gel containing Fe ions in pure water to increase the pH. I then froze the phase separated DN gels in liquid nitrogen. The water in the phase separated DN gels was replaced by acrylic resin (London Resin white, medium) using an automated freeze-substitution system (EM AFS2, Leica Microsystems, Germany) and then cut into 100 nm sections. The sections were observed by transmission electron microscopy (TEM, H-7650, Hitachi, Japan). The acceleration voltage of the electron gun for observation was set at 100 kV.

5.3 Experimental section

5.3.1 Comparing the electric potential profiles and TEM image of phase separated DN gels

The phase separation DN gel samples used for the Donnan potential and TEM measurements were each cut out from a single gel sheet. I compared the optical clarity of phase separation DN gels and their microscopic structure with changing dioxane content during synthesis. As shown in Figure 5.1 (a), the phase separation DN gels were transparent when the dioxane weight fraction was $r \leq 0.3$, while it became cloudy when $r \geq 0.4$. I confirmed this by TEM images and measured the inside of the phase separated DN gels by microelectrode technique for r = 0, 0.3, 0.4, and 0.54. The poly(NaAMPS) chains of the phase separated DN gels were stained by Fe mineralization and observed by TEM in Figure 5.1 (b). These TEM images showed that there was no aggregation of the poly(NaAMPS) chains with dioxane weight fractions from 0 and 0.3. Furthermore, increasing the dioxane concentration to r = 0.4, phase separation occurred, resulting in a dense phase with a higher concentration of poly(NaAMPS) chains and a sparse phase with a lower concentration of poly(NaAMPS) chains, with an average dense phase size of 2.0 ± 0.6 μm at r = 0.4 and a dense phase with high contrast at r = 0.54. Here, the dense phase size is expressed as mean ± the standard deviation (Number of samples: 50). Also, according to the discussion by Kiyama et al.[7], the thickness of the phase separation DN gels shrinks by about 15% in length during the TEM sample preparation process. Therefore, the dense phase size obtained by TEM observation is the size of the phase separation DN gels after shrinkage. Assuming the same shrinkage rate for this phase separated DN gel, and correcting for the shrinkage, the size of the dense phase is 2.4 ± 0.7 μm for r = 0.4 and 5.2 ± 1.2 μm for r = 0.54, respectively.

The dense phase that contains a higher content of poly(NaAMPS) chains has more negative charge, and the resulting electric potential is larger in the negative direction. From this point on, the absolute value of the electric potential is used when comparing the magnitude of the electric potential. The results of microelectrode technique were shown in Figure 5.1 (c). The fluctuation of the electric potential profile was slight for r = 0 to 0.3. In contrast, the fluctuation of the electric potential profile from r=0.4 to 0.54 was more significant. Considering that the potential is larger in the dense phase and smaller in the sparse phase, the electric potential range of about -100 mV represents the sparse polyelectrolyte phase, and the electric potential range of about -200 mV represents the dense polyelectrolyte phase. This trend of electric potential fluctuation was consistent with the presence or absence of phase separated structures in the gel photographs and TEM images. Microelectrode technique possesses sufficient resolution that I can clearly measure electric potential changes that are related to the local structure.

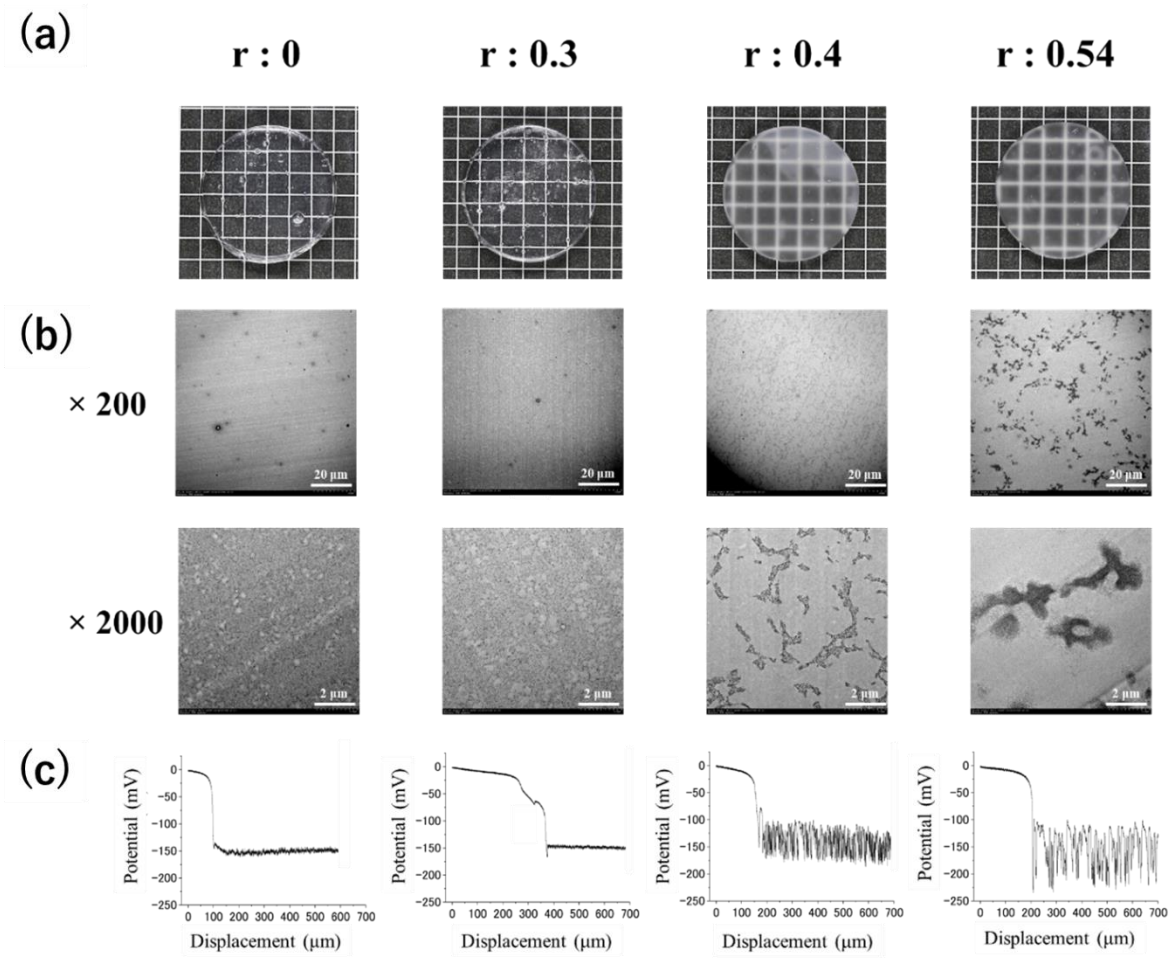

Fig. 5-1 TEM and microelectrode technique evaluation of phase separated DN gels prepared in dioxane/water mixture solvents of various dioxane weight fraction, r. (a) Photographs of the phase separated DN gels after swelling. (b) TEM images of the phase separated DN gels at different magnifications. (c) Potential profiles of phase separated DN gels measured by microelectrode technique.

5.3.2 Calculate the polymer concentration of phase separation DN gels

As mentioned in Section 2.3.1, since microelectrode technique observe on a scale (μm scale) that is sufficiently larger than the mesh size of the hydrogel (nm scale), the electric potential obtained by microelectrode technique reflects the average value of the counterion concentration within the measurement range of the capillary tip. Also, this measurement range is sufficiently larger than the Debye length of the counterions around the fixed ion on the polyelectrolyte chain. Therefore, the charge of the polyelectrolyte network and the counterions maintain electrical neutrality, and the average counterions concentration over a volume of the detection range is considered to be equal to the charge density of the polyelectrolyte network (polymer concentration).

Then, I calculated the polymer concentration, which is molar concentration of fixed charge of poly(NaAMPS) inside the hydrogel from the obtained electric potential profile. The polymer concentration and counterions concentration are considered to correspond 1:1 because the charges of the polyelectrolyte chains and counterions are electrically neutral in this experimental system. Therefore, I calculated the counterion concentration (C_g) around the polyelectrolyte chain inside the gel according to equation (2.6)[8,9], which can be re-written for simplicity as

$$C_g = \frac{C_s \gamma_s}{10^{\frac{zF\Phi_D}{2.3RT}}} \times \frac{1}{\gamma_g} = \frac{a_g}{\gamma_g} \qquad (5.1)$$

Here, C_g is the polymer concentration (charge density of polyelectrolyte network), or the counterion concentration around the polyelectrolyte network inside the polyelectrolyte hydrogel , C_s is molar concentration of counterion in the reference solution, a_g is the activity of counterion around the polyelectrolyte network inside the polyelectrolyte hydrogel, a_s is the activity of counterion in the electrolyte solution, γ_s is the activity coefficient of ions in the

electrolyte solution, γ_g is the activity coefficient of ions in the polyelectrolyte hydrogel, Φ_D is the Donnan potential, R is gas constant, T is absolute temperature, z is ionic valence, F is Faraday constant.

In this study, 10^{-5} M $NaCl_{aq}$ was used as the reference solution, so $C_s = 10^{-5}$ and z = 1. The activity coefficients of ions in the $NaCl_{aq}$ with such a low concentration could be considered as an ideal solution, so I assumed $\gamma_s \approx 1$. Here, the activity coefficient of the effective counterions (γ_g) should change with the polymer concentration in the phase separated structure. It was assumed that the activity coefficient in the concentrated phase of the phase separated DN gel decreases because the relative dielectric constant around the polymer chains decreases, and the activity coefficient also decreases[10]. Conversely, the activity coefficient in the sparse phase was assumed to be larger. The method to measure the activity coefficient in the dense phase and the sparse phase has not yet been established. Therefore, I calculated the average values of the activity coefficients as the activity coefficients of the counterions near the fixed ions inside the hydrogel, using the mean polymer concentration calculated from the gel's swelling ratio (Q) and the mean activity obtained from microelectrode technique. Since the gel swells isotopically, the cube of the ratio of the thickness of the gel after phase separated DN gelation and swelling to the thickness of the poly(NaAMPS)gel immediately after preparation was used as the swelling ratio of the gel (Q).

$$Q = \left(\frac{t_{DN,sw}}{t_{1st,as-pre}} \right)^3 \quad (5.2)$$

$$\overline{C_{sw}} = \frac{C_{ini}}{Q} \quad (5.3)$$

$$\overline{\gamma_g} = \frac{\overline{a_g}}{\overline{C_{sw}}} \quad (5.4)$$

Here, $t_{DN\ ,sw}$ is the thickness of the phase separated DN gel after swelling, and $t_{1st,as-pre}$ is the thickness of the poly(NaAMPS) gel before swelling in DMAAm solution. Since the charge of the PDMAAm gel, which is a neutral gel, has no effect on the Donnan potential measurement, the swelling ratio Q is the volume ratio of the poly(NaAMPS) gel. In addition, because the gel swells isotropically, the cube of the thickness change of the gel was used as the swelling ratio (Q). C_{ini} is the prepared monomer concentration. $\overline{C_{sw}}$, $\overline{a_g}$, and $\overline{\gamma_g}$ denote the average of the polymer concentration, the activity, and the activity coefficient, respectively.

$$C_g \simeq \frac{a_g}{\overline{\gamma_g}} \quad (5.5)$$

Assuming that the $\overline{\gamma_g}$ is equal to γ_g, the counterion concentration C_g for a fixed charge of the polyelectrolyte network can be calculated using equation (6), using the concentration of effective counterions around the local polyelectrolyte chains (a_g) obtained from the electric potential measurement. This result means that it is possible to estimate the polymer concentration from the Donnan potential, the preparation concentration of NaAMPS monomer and the swelling ratio in this experimental system.

Using Equation (5.4), the average activity coefficients were calculated for the cases where phase separation was not observed (r=0) and where phase separation was confirmed (r=0.4, 0.5, 0.54). The results are summarized in Table 5-1. The PNaAMPS/PDMAAm DN gel with dioxane weight fraction r = 0 showed no internal phase separated structure. The obtained $\overline{\gamma_g}$ was 0.17, which is reasonable because it is close to the activity coefficient $\overline{\gamma_g}$ of 0.22 for the DN gel of PAMPS/PAAm in the study by Nakajima et al[10]. The $\overline{\gamma_g}$ values at r = 0.4, 0.5, and 0.54 for gels with a phase separated structure are assumed to be different for the dense and sparse phases. The method to measure the activity coefficients in the phases with different

concentrations has not yet been established. Therefore, I used the mean hydrogel activity coefficient calculated by the same method to obtain the activity coefficient for r = 0. The value of the activity coefficient $\overline{\gamma_g}$ obtained by this method may differ from the actual activity coefficient and therefore the polymer concentrations of the converted dense and sparse phases may also differ from the actual concentrations. However, since the difference does not affect the trend of polymer concentration change due to the difference in dioxane weight fraction, it can be sufficiently considered the actual polymer concentration.

Table 5-1.

Dioxane weight fraction r	Swelling ratio Q	Average polymer concentration $\overline{C_{sw}}$	Average activity $\overline{a_g}$	Average activity coefficient $\overline{\gamma_g}$
0	50	2.0×10^{-2} M	3.4×10^{-3} M	0.17
0.4	101	1.0×10^{-2} M	3.2×10^{-3} M	0.32
0.5	60	1.7×10^{-2} M	2.8×10^{-3} M	0.16
0.54	40	2.5×10^{-2} M	7.8×10^{-3} M	0.31

5.3.3 Polymer concentration and dense phase sizes of phase separated DN gels

Figure 5.2 (a,b,c,d) showed the electric potential profiles as a function of displacement for r = 0, which is the reference in pure water, and r = 0.4, 0.5, and 0.54, where phase separation was confirmed and converted to activity and polymer concentration according to equation (5.5). The mean polymer concentration at each dioxane weight fraction obtained from the concentration profile was shown in Figure 5.2 (e,f). The red dots in the figure represent the mean polymer concentration in the dense phase, the blue dots represent the mean polymer concentration in the sparse phase, and the black dots represent the mean polymer concentration in the gel without phase separation. The mean polymer concentration in the dense phase was 2.8×10^{-2} M at r = 0.4, 1.3×10^{-1} M at r = 0.5, and 1.8×10^{-1} M at r = 0.54, respectively. The mean polymer concentration in the sparse phase was 2.5×10^{-3} M at r = 0.4, 2.0×10^{-4} M at r = 0.5, and 2.1×10^{-4} M at r = 0.54, respectively. We see that as the dioxane weight fraction increases, the concentration of the dense phase increases, and the concentration of the sparse phase decreases. The concentration of the dense phase was found to be 85 times that of the sparse phase in the highest density region. This result is consistent with the trend observed by contrast shading in the TEM images, indicating that, in contrast to the conventional qualitative measurement method, microelectrode technique can continuously and quantitatively measure the local polymer concentration in a phase separated gel.

According to the discussion by Guo et al. [16], the counterion concentration (C^+, C_g) in the sparse phase is approximately 2.0×10^{-3} M according to Figure 5.2 (f), and the polymer concentration (C_p^-, C_{sw}) is also the same based on the electrical neutrality condition according to equation (5.7). Since the reference solution (C_s) concentration is 10^{-5} M, the co-ion concentration (C^-) is 5.0×10^{-8} M according to equation (5.8).

$$C^+ = C^- + C_p^- \quad (5.7)$$

$$C_s^2 = C^+C^- \quad (5.8)$$

Since the co-ion concentration is sufficiently low compared to the fixed ion concentration, the Debye length in the sparse phase is estimated to be equal to the Debye length in pure water at pH 6.5 (about 540 nm). Since the counterion concentration (C^+) in the dense phase is more than 2.8×10^{-2} M according to Figure 5.2 (f), the co-ion concentration (C^-) is less than 3.6×10^{-9} M and can be ignored. Therefore, the Debye length of the dense phase is about 540 nm, similar to the Debye length of the sparse phase.

TEM observation revealed the formation of a sea-island structure. The dense phase's size is defined as the area where the concentration is higher than the base concentration, red line, based on the concentration of the sparse polyelectrolyte chains in each concentration profile, as shown in Figure 5.2 (g,h). The base concentration of the polymer in each concentration profile was 2.5×10^{-3} M at r = 0.4, 2.0×10^{-4} M at r = 0.5, and 2.1×10^{-4} M at r = 0.54, respectively.

The dense phase sizes obtained from each concentration profile were shown in Figure 5.2 (i) as box plots. Here, the box represented the 25th-75th percentile, the whiskers represented the 10th-90th percentile interval, and the straight line in the box represented the median. The results showed that the dense phase size obtained from microelectrode technique at r = 0.4 is about 5 μm, at r = 0.5 is about 14 μm, and at r = 0.54 is about 20 μm. Therefore, as the dioxane concentration increases, the dense phase size also increases.

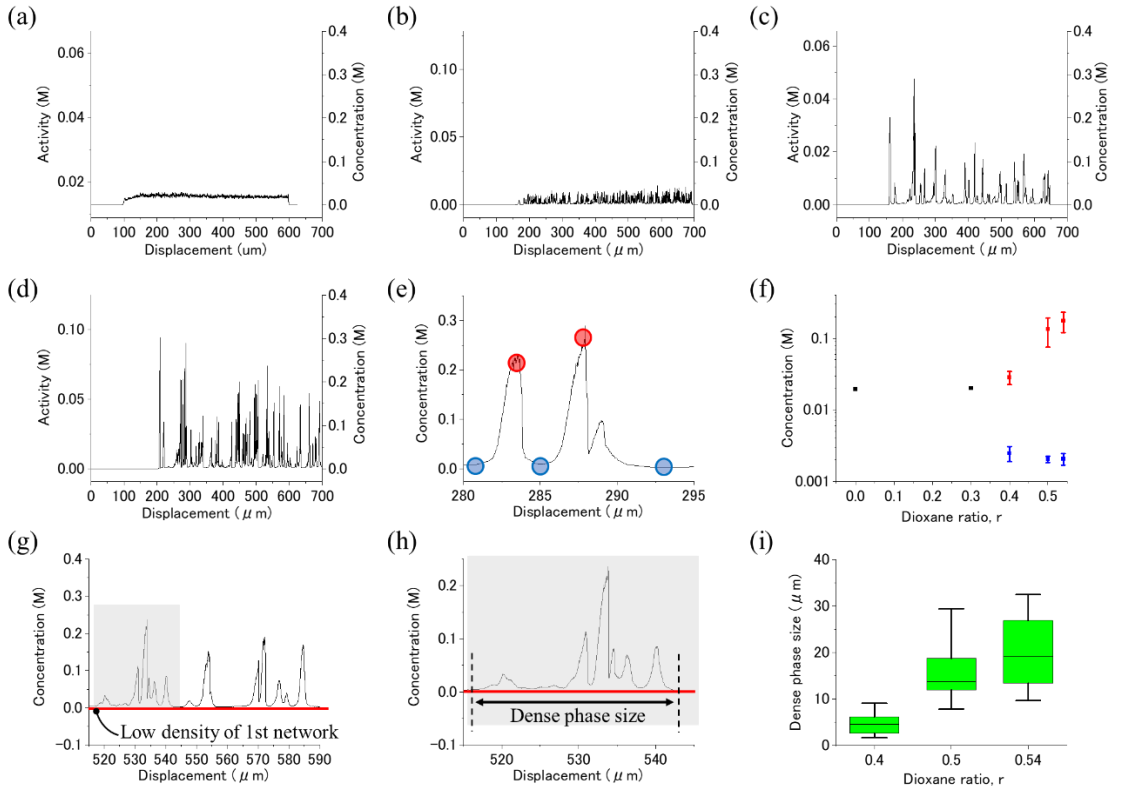

Fig. 5.2 Concentration profiles and dense phase size of separated DN gels obtained from microelectrode technique. (a,b,c,d) Polymer concentration profiles of phase separation DN gels. I converted the phase separated DN gels' electric potentials obtained by microelectrode technique into polymer concentration. Vertical axes: activity (M, left axis) or polymer concentration (M, right axis), horizontal axis: displacement (μm). Dioxane weight fractions r to precursor solution: (a) 0, (b) 0.4, (c) 0.5, (d) 0.54. (e) Polymer concentration of dense and sparse phases in the phase separated DN gel at r =0.54. Red and blue points are maximum and minimum concentrations, respectively. (f) The polymer concentration in the dense phase (red) and the mean polymer concentration in the sparse phase (blue) as a function of dioxane weight fraction. (g) Relationship between electric potential profile and dense phase size. The red line is the baseline of the sparse phase's polymer concentration. (h) Definition of the size of the dense phase based on the sparse phase's polymer concentration the part where the polyelectrolyte network is sparse). r = 0.54 is shown as an example. (i) Dense phase size in

phase separated DN gels. The box plots for the 25th-75th percentiles were shown with the dense phase size on the vertical axis and the dioxane weight fraction (r) on the horizontal axis. Here, the whiskers indicate the 10th-90th percentile interval, and the straight line in the box represents the median. The sparse phase's polymer concentration for each concentration profile was 2.4×10^{-3} M at r = 0.4, 2.0×10^{-4} M at r = 0.5, and 2.1×10^{-4} M at r = 0.54.

5.3.4 Estimation of spatial resolution of MET through comparison of dense phase sizes measured by TEM and MET

I considered the differences in the dense phase size as measured by TEM and microelectrode technique. The corrected dense phase size obtained from the TEM image was 2.4 ± 0.7 μm at r=0.4, and 5.2 ± 1.2 μm at r = 0.54. respectively. In contrast, the dense phase size obtained from microelectrode technique was about 5.0 ± 2.8 μm at r = 0.4 and 20 ± 8.6 μm at r = 0.54. Thus, the size of the dense phase obtained by microelectrode technique is several times larger than that obtained from the TEM image. To understand why the dense phase size observed by microelectrode technique and TEM is different, I need to know the detection range and spatial resolution of microelectrode technique. Figure 5.3 (a) shows a magnified view of the electric potential profile at r = 0.4, where the concentration peak of the dense phase appears at 560 μm in displacement, then returns to the concentration range of the bulk hydrogel, and then a new concentration peak of the dense phase appears at 564 μm. Therefore, the maximum detection range of microelectrode technique is obtained by subtracting the length of the reference concentration region between the two concentration peaks from the length between the two concentration peaks. In this experiment, the detection range was determined to be less than 1.5 μm. As described **3-2-2**, if the concentration change is more than 2% in this experimental system, it can distinguish the concentration measurement from white noise. Therefore, it can be concluded that the concentration changes significantly exceeding the noise can be divided into two peaks in the 564-566 μm part of Figure 5.3 (a). The distance between these two peaks is about 0.8 μm. Therefore, it was determined that the spatial resolution of microelectrode technique is less than 0.8 μm (sub-micrometer scale).

Based on this assumption, I consider why the dense phase size in microelectrode technique is larger than that in TEM. The TEM sample is a thin layer section with a thickness of 100 nm thickness, but due to the cutting process all depth information is lost. For example, if the dense phase is present, as shown in Figure 5.3 (b,c), it is impossible to know if the size represents the maximum width of the dense phase or just some portion of the total phase. In contrast, the microelectrode technique detection range is considered to be the range where the KCl_{aq} leaks from the tip of the capillary, which means that the detection range is spatially extended, as shown in Figure 5.3 (d,e). Besides, since the capillary is advanced at a constant speed, the microelectrode technique can scan from the top of the dense phase to the bottom. However, because of its high sensitivity, the microelectrode technique recognizes both the entrance into, as well as the exit out of the dense phase. Therefore, the observed dense phase size may be expressed as the total size of the diameter of the detection range and the original size of the dense phase. When the distance between one dense phase and the next dense phase on the measurement line is less than the size of the detection range of the microelectrode technique, it is difficult to distinguish whether the obtained signal is one dense phase with different parts of concentration inside or multiple dense phases with different concentrations. Based on this analysis, microelectrode technique provides us with a method to more accurately measure the local size and shape of phase separated hydrogels.

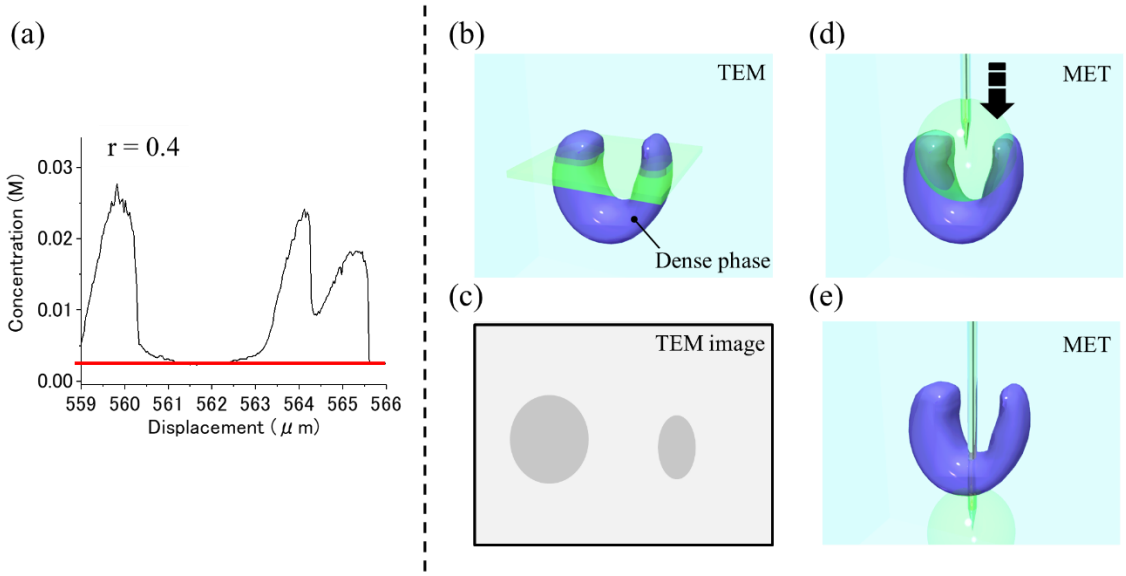

Fig. 5.3 (a) The estimation of detection range and spatial resolution of microelectrode technique. Characteristic peaks based on the concentration profile of the DN gel at r = 0.4. A partially enlarged view of the electric potential profile at a dioxane weight fraction of 0.4 is shown. The red line represents the base concentration. (b) The green rectangle shows the measurement cross-section of TEM. (c) The illustration shows a TEM image of the dense phase. (d)-(e) The green sphere shows the detection range of microelectrode technique.

5.4 Conclusion

The improved microelectrode technique successfully measured the sizes of the dense and sparse phases within the phase separated DN gel, allowing for the observation of the spatial distribution of polyelectrolyte network. Furthermore, using microelectrode technique, I successfully quantitatively measured local concentrations within the polyelectrolyte hydrogel and the average activity coefficients of counterions, which were not achievable with other conventional measurement methods. This revealed that the polymer concentration in the phase separated dense phase can be up to 85 times higher than that in the sparce phase. In addition, from the polymer concentration profile of electrolyte polymer in the phase separated DN gel, I estimate that the microelectrode technique detection range is less than 1.5 μm and the spatial resolution is less than 0.8 μm.

From the above, it can be concluded that microelectrode technique is a powerful tool for locally and quantitatively measuring the internal structure and polymer concentration of polyelectrolyte hydrogels with sub-micrometer scale heterogeneity without the need for pre-treatments such as freeze-drying or staining. This method can be applied to cells and organs *in vivo*, due to their similarities with polyelectrolytes. Enabling the *in-situ* determination of internal structures of biomaterials could have important implications towards characterization of damaged and diseased tissues on the local scale.

5.5 References

1. Kawauchi, Y.; Tanaka, Y.; Furukawa, H.; Kurokawa, T.; Nakajima, T.; Osada, Y.; Ping Gong, J. Brittle, Ductile, Paste-like Behaviors and Distinct Necking of Double Network Gels with Enhanced Heterogeneity. In *Journal of Physics: Conference Series*; Institute of Physics Publishing, **2009**; Vol. 184.
2. Nishimura, T.; Guo, H.; Kiyama, R.; Katsuyama, Y.; Gong, J.P.; Kurokawa, T. In Situ Evaluation of the Polymer Concentration Distribution of Microphase-Separated Polyelectrolyte Hydrogels by the Microelectrode Technique. *Macromolecules* **2021**, 54, 10776–10785.
3. Gong, J. P.; Katsuyama, Y.; Kurokawa, T.; Osada, Y. Double- Network Hydrogels with Extremely High Mechanical Strength. Adv. Mater. **2003**, 15, 1155−1158.
4. Yasuda, K.; Gong, J. P.; Katsuyama, Y.; Nakayama, A.; Tanabe, Y.; Kondo, E.; Ueno, M.; Osada, Y. Biomechanical Properties of High-Toughness Double Network Hydrogels. *Biomaterials* **2005**, *26* (21), 4468–4475.
5. Guo, H.; Kurokawa, T.; Takahata, M.; Hong, W.; Katsuyama, Y.; Luo, F.; Ahmed, J.; Nakajima, T.; Nonoyama, T.; Gong, J. P. Quantitative Observation of Electric Potential Distribution of Brittle Polyelectrolyte Hydrogels Using Microelectrode Technique. *Macromolecules* **2016**, *49* (8), 3100–3108.
6. Guo, H.; Hong, W.; Kurokawa, T.; Matsuda, T.; Wu, Z. L.; Nakajima, T.; Takahata, M.; Sun, T.; Rao, P.; Gong, J. P. Internal Damage Evolution in Double-Network Hydrogels Studied by Microelectrode Technique. *Macromolecules* **2019**, *52* (18), 7114–7122.

7. Kiyama, R,; Yoshida, M,; Nonoyama, T,; Tomas,S,; Jinnai, H,; Kurokawa, T,; Nakajima, T,; Gong, J. P. Nanoscale TEM Imaging of Hydrogel Network Architecture, *Adv.Mater.* **2022**, 2208902-2208902
8. Crothers, D. E. a. D., Physical Chemistry with applications to the life sciences. 1979; p. p 385.
9. Donnan, F. G. Theorie der Membrangleichgewichte und Membranpotentiale bei Vorhandensein von nicht dialysierenden Elektrolyten. Ein Beitrag zur physikalisch-chemischen Physiologie. *Z. Electrochem* **1911**,17, 572
10. Aonuma, H.; Nagayama, T.; Takahata, M. *Distribution of Autofluorescent Cell Bodies in the Crayfish Central Nervous System*; **1996**.
11. Nakajima, T.; Chida, T.; Mito, K.; Kurokawa, T.; Gong, J. P. Double-Network Gels as Polyelectrolyte Gels with Salt-Insensitive Swelling Properties. *Soft Matter* **2020**, *16* (23), 5487–5496.

Chapter 6 A spatial analysis of the damage zone in double network hydrogel using microelectrode technique

This work was reprinted with permission from " Nishimura, T.; Guo, H.; Katsuyama, Y.; Masahiro, Y.; Gong, J.P.; Kurokawa, T. Spatial Analysis of the Damage Zone in Double Network Hydrogel Using the Microelectrode Technique Macromolecules 2024, online. Copyright 2024 American Chemical Society." This chapter has been modified from its original form.

6.1 Introduction

Up to **Chapter 5**, it has been demonstrated that the improved microelectrode technique can measure the sub-micrometer scale heterogeneous structure of polyelectrolyte hydrogels[1]. In this chapter, as an example of analyzing the internal heterogeneous structure of polyelectrolyte hydrogels using the capabilities of the microelectrode technique, I introduce to observe the internal structure of polyelectrolyte network in the damage zone of DN gel and to infer the fracture behavior based on the sacrificial bond principle.

As shown in Section 2-1-4 of **Chapter 2**, double network hydrogels (DN gels) have an interpenetrating network structure consisting of a hard and brittle first network and a soft and well-stretchable second network. Typical DN gels composed of a polyelectrolyte first network and a neutral polymer second network boast significantly higher strength and toughness than general high water-containing gels. Since DN gels are materials that can control water retention and provide biocompatibility, they have been attracting attention as biomaterials and industrial

materials in recent years[2-4]. The reason for the superior high-strength properties of DN gels has been explained as follows. The first network preferentially ruptures when subjected to large deformation, causing energy dissipation. At the same time, the second network stretches extensively and ruptures the neighboring first network, causing even more significant energy dissipation. This is the so-called sacrificial bond principle[5-8].

The region where the first network is preferentially ruptured (the red area in Figure 6.1) is called the "damage zone"[9-12]. The first network structure of the damage zone plays a crucial role in considering the high toughness of the DN gel. Previous research had reported the relationship between the size of the damage zone near the crack tip in the X-Y plane of Figure 6.1, as determined by optical or fluorescence microscopic observation, and the energy dissipation by mechanical characterization[13-15]. Additionally, speculation about the rupture structure of the first network during DN gel destruction has been made based on cycle testing during DN gel failure and X-ray small-angle scattering results[16,17]. However, to thoroughly understand the high toughness mechanism of DN gel, it is essential to obtain a continuous distribution of DN gel's first network structure in three-dimensional space. Existing reports have often been limited to discussions in the X-Y plane or have relied on judgments from averaged information within the measurement area. Therefore, the observation of the first network's structure and spatial distribution in the Z-axis direction within the damage zone has yet to be achieved. The primary challenge in achieving this lies in the technical difficulty of establishing a method to measure the hydrogel's structure in the Z-axis direction.

In this chapter, I adopted an improved microelectrode technique to measure the Donnan potential distribution in the damage zone around the crack tip of a DN gel[1,18-20]. The spatial

resolution of this improved method is approximately 800 nm, which is significantly larger than the gel network size. Therefore, under electrically neutral conditions, it is reasonable to assume a 1:1 correspondence between measurable counterions and the fixed macroions of the first network.

In the case of a DN gel, the ruptured region of the first network has a locally increased swelling ratio and a decreased charge density distribution of first network, so called “polymer concentration.” Therefore, this study aimed to quantitatively determine the concentration of polyelectrolytes in the damage zone, visualize the extent of damage, and obtain the spatial distribution of the first network within the damage zone of DN gel.

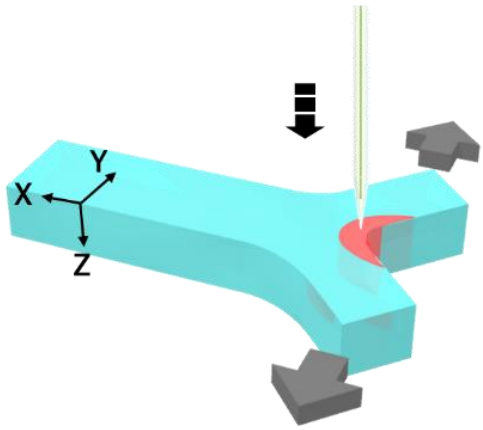

Fig. 6.1. An illustration of the damage zone created when tearing DN gel, along with the insertion of a microelectrode in the Z-axis direction for microelectrode technique. The red area represents the damage zone. The gray arrows represent the tearing direction. The direction of crack propagation when torn is defined as the X-axis, the tearing direction as the Y-axis, and the thickness direction of the gel as the Z-axis. The microelectrode is an inserted image and differs from the actual size.

6.2 Experimental section

6.2.1 Materials

2-Acrylamido-2-methylpropanesulfonic acid sodium salt (NaAMPS) was provided courtesy of Toa Gosei Co., Ltd. N, N-Dimethylacrylamide (DMAAm), N, N′-Methylenebis(acrylamide) (MBAA), 2-oxoglutaric acid (OA) and sodium chloride (NaCl) were purchased from FUJIFILM Wako Pure Chemical Industries, Ltd. All materials were used as received.

6.2.2 Synthesis of DN gels and immersed in salt solution[3,4]

I prepared DN gels using NaAMPS in the first network and DMAAm in the second network. Negatively charged monomer (NaAMPS: 1 M), cross-linker (MBAA: 4 mol% relative to NaAMPS concentration), and initiator (OA: 0.1 mol% relative to NaAMPS concentration) were dissolved in pure water. The solution was poured into a glass mold of two soda-lime glass plates (thickness : 3 mm) by a U-shaped silicone rubber sheet (thickness: 1.5 mm). The mold was irradiated with UV light (365 nm; 4 mW/cm^2) for 8 hours under an argon atmosphere. The poly(NaAMPS) gels were immersed in an aqueous solution of neutral monomer (DMAAm: 2 M), cross-linker (MBAA: 0.02 mol% relative to DMAAm concentration), and initiator (OA: 0.01 mol% relative to DMAAm concentration) at room temperature for 2 or 3 days. After immersion, the poly(NaAMPS) gel was sandwiched between two soda-lime glass plates. The gels were irradiated with UV light (365 nm; 4 mW/cm^2) for 9 h under an argon atmosphere. The prepared hydrogels were immersed in pure water, and the soaking water was changed daily for about one month to remove residual monomer and initiator. After that, the DN gel, swollen to 4 mm thick, was immersed in 10^{-5} M $NaCl_{aq}$ for over two days to reach equilibrium.

6.2.3 Tearing test of the DN gel

In order to observe in detail, the first network structure in the damage zones formed during the tearing process, samples including the unfractured zone to the completely fractured zone, were prepared and used for the Donnan potential measurement by the following method. DN gel with a thickness of 4 mm was cut into trouser-shaped hydrogel specimens with an overall dimension of 5 cm × 7.5 cm and a 1 cm cut near the center of the short side using a laser cutter (VLS4.75,Universal laser systems). Tearing tests were performed with an Instron (Instron 5965, Instron Co., USA). Both ends of the test specimen were fixed to jigs, and a Mode I type (opening mode) tensile test was performed in the Y-axis direction of Figure 6.1 at a speed of 100 mm/min. When in the steady-state crack propagation at a constant stress, the strain was stopped, and the gel specimen removed from the jigs was immersed in a 10^{-5} M $NaCl_{aq}$ until equilibrium swelling was reached again.

6.2.4 Electric potential measurement of the damage zone of the DN gel[1,19,20]

The DN gel with completed solvent replacement is impregnated into a fresh 10^{-5} M $NaCl_{aq}$ container. The container was fixed on an XY stage (LD-6042-C7, Chuo Seiki) so that it could be moved in 1 μm increments in the direction of crack propagation (X-axis direction). The capillaries were made by stretching a glass tube (BF100-75-15, Sutter, USA) using a Puller (P-2000, Sutter, USA). A capillary was inserted in the Z-axis direction of the damage zone in Figure 6.1 at a speed of 0.8 μm/sec to obtain electric potential profiles along the thickness direction of the hydrogel. Electric potential measurements were performed in 50 μm steps back and forth from an initial measurement point near the crack tip until there was no change in electric potential, or the electric potential could no longer be measured.

6.2.5 Imaging of the DN gel crack tip

After the electric potential measurement, I observed the hydrogel near the crack tip under a microscope. (Eclipse LV100N POL, Nikon Co., Japan), and it was confirmed that the electrode could measure the crack vicinity

6.3 Result & Discussion

6.3.1 Imaging of the DN gel crack tip

The result of observing the crack tip of the DN gel with a microscope after measuring the electric potential using microelectrode technique is shown in Figure.2 (a). The positions where the electric potential was measured are observed as equal intervals of points on a straight line. This is because when measuring the hydrogel's electric potential, the network is locally broken as the electrode penetrates, and the areas after the measurement re-swell. From this point onwards, the crack tip in Figure 6.2 (b) was used as the origin. The distance from the crack tip to the closest measurement point, as determined from the microscope measurements, was approximately 35 μm.

Figure 6.2 (a,b) shows that radial wrinkle-like regions near the crack tip were observed at less than 235 μm, similar to those by Liang et al[13]. They observed that the DN gel was fractured heterogeneously perpendicular to the stretching direction in the vicinity excluding the immediate area around the crack tip. Similarly in our case, a wrinkle-like region is observed near the crack tip of the DN gel. This is thought to be because the first network was preferentially ruptured, and the local swelling changed the refractive index of the ruptured area, making it appear as a wrinkle-like region. Here, the luminance changes in the crack seen in the lower right part of Figure 6.2 (a,b) is due to light scattering and reflection and does not represent the actual structure of the crack.

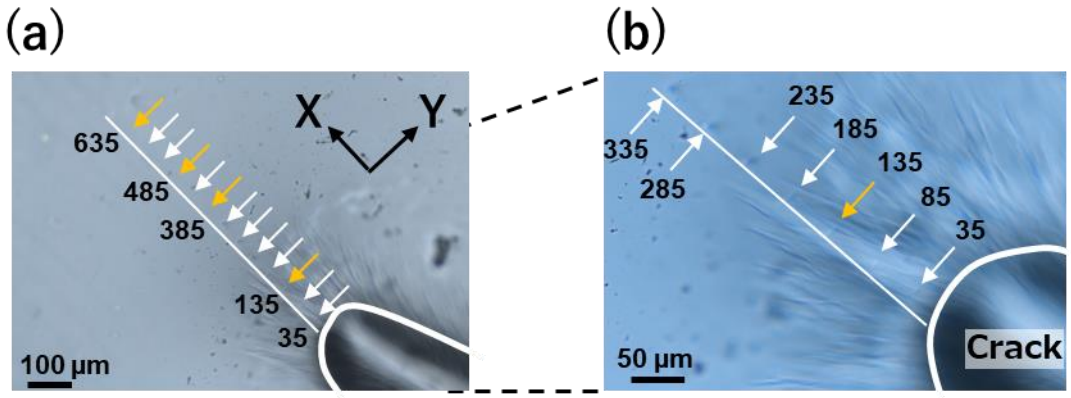

Fig. 6.2 (a) Microscopic image of the area around the crack tip. Arrows indicate the measurement points. The yellow arrows indicate the areas where the electric potential data are shown in the text. (b) Enlarged microscopic image of the area around the crack tip.

6.3.2 Electric potential profiles and electric potential histograms in the damage zone of tearing DN gel

The obtained electric potential profiles can be broadly categorized into three groups, and representative electric potential profiles (at positions 135 μm, 385 μm, 485 μm, and 635 μm from the crack tip) are selected and presented in Figure 6.3 (a,b,c,d,e). Additionally, the electric potential profiles at all positions are provided in Figure 6.4. The vertical axis represents the electric potential (mV), and the horizontal axis represents the distance advanced by the capillary (= displacement, μm). Figure 6.3 (f,g,h,i,j) shows a histogram of the variation of the electric potential inside the hydrogel along the Z-direction in each position. The horizontal axis represents the electric potential (mV), and the vertical axis represents the probability of each electric potential zone when the sum of the probability for all classes in the histogram is set to 1, with a bin value of 2 mV. Gaussian fitting is applied to the histograms, and the profiles of red, green, and blue represent those profiles.

From the microscopic images in Figure 6.2, it can be observed that the region between positions 35 μm and 185 μm corresponds to a "wrinkle-like region," where the electric potential is significantly smaller compared to the bulk. This suggests that the first network is extensively ruptured in this area. On the other hand, in positions where the wrinkle-like region is not observed, two types of profiles can be identified. The region from 235 μm to 585 μm exhibits rectangular wave-like electric potential profiles, while positions 635 μm and beyond show electric potential profiles similar to the bulk. In other words, in positions without a wrinkle-like region, there are areas where the first network has ruptured partially in the Z-axis direction and areas where the first network has remained unruptured.

According to the studies by Liang et al.[13], they observed and defined three distinctive zones: hardening zone, yield zone, and preyield zone, near the crack tip when DN gel is torn, and only in the yield zone, a wrinkle-like region was observed. Since the DN gel used in this study does not cause hardening, the hardening zone is not mentioned hereafter. Therefore, in the context of the damage zone within the hydrogel, where the electric potential exhibits non-constant behavior along the z-axis in Figure 6.1, I designate the position from 35 μm to 185 μm at Figure 6.3 (a), where the wrinkle-like region is observable in Figure 6.2 (a,b), as the “yield zone”. Conversely, the position from 235 μm to 585 μm at Figure 6.3 (b,c), where a stepwise change in electric potential occurs but the presence of a wrinkled area cannot be confirmed, is referred to as the “preyield zone”. The unruptured regions of the first network at Figure 6.3 (d) characterized by a consistent electric potential along the Z-axis in Figure 6.1 from position 635 μm and beyond are referred to as "undamage zone”.

In Figure 6.3 (f-j), two electric potential peaks are present in the histogram of the preyield zone, which means that the electric potential is binarized. In the subsequent yield zone, these electric potential peaks become closer to each other and nearly homogeneous. In addition, it can be confirmed that the electric potential tends to shift to the lower side as it approaches the crack tip from the undamage zone. Based on these findings, the following conclusions can be drawn : In the preyield zone, the first network in the hydrogel segregates into parts where it preferentially ruptures and parts where it does not along the z-axis. As one approaches the crack, the unruptured network progressively undergoes rupture. In the yield zone, the rupture of the first network extends throughout the entire region along the z-axis.

35 μm
～
185 μm

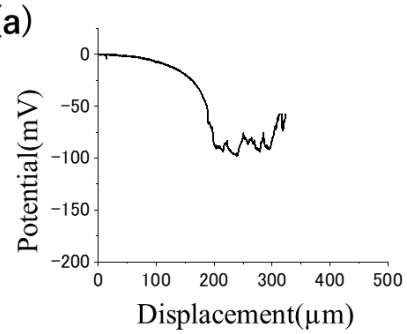

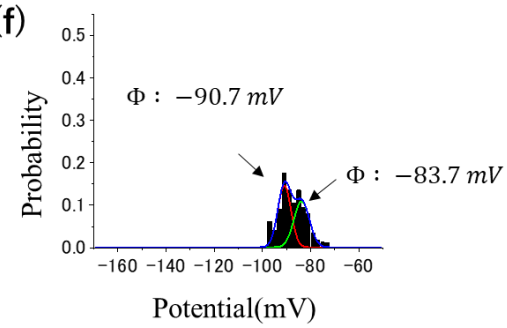

235 μm
～
585 μm

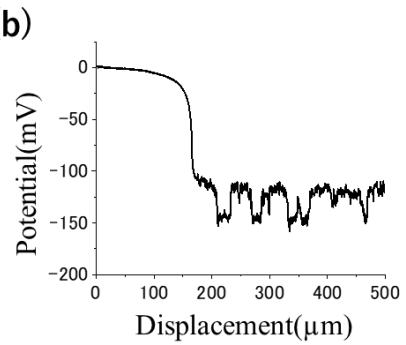

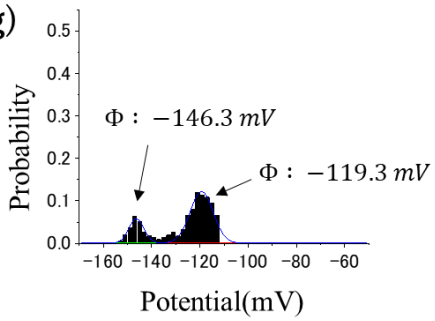

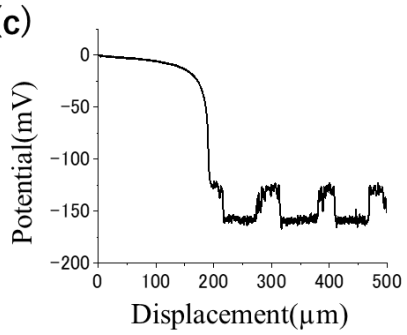

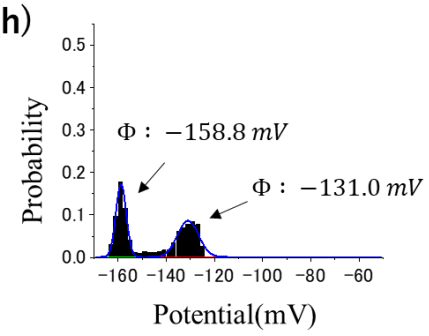

635 μm
～

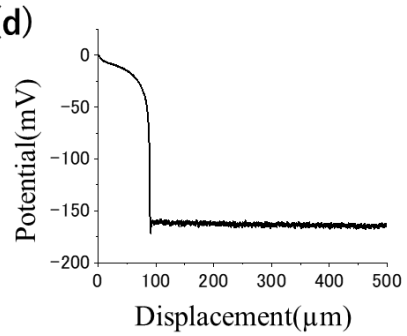

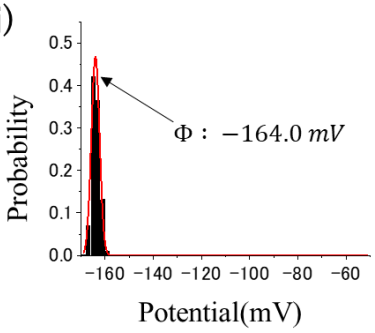

Bulk

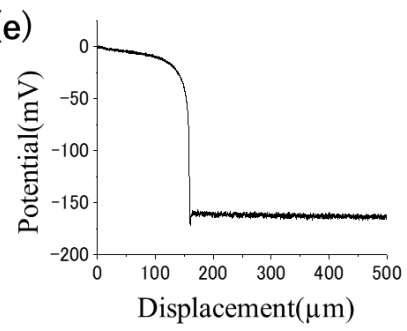

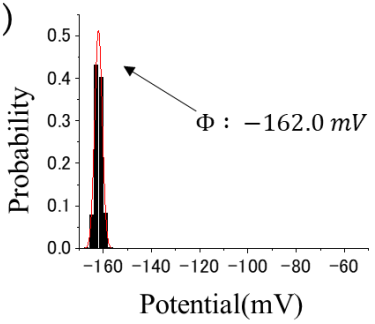

Fig. 6.3 (a-e) Electric potential profiles for presentative positions in the damage zone and in bulk. The vertical axis represents the electric potential, and the horizontal axis represents the distance advanced by the capillary. The numbers on the left of the figures are positions from the crack tip. (f-j) Histogram of electric potential variation expressed as 2 mV bin values corresponding to (a-e). The vertical axis represents the presence ratio, and the horizontal axis represents the electric potential. The profiles of green, red, and blue are obtained through Gaussian fitting, and they are utilized to estimate the electric potential peaks. Φ represents the peak electric potential.

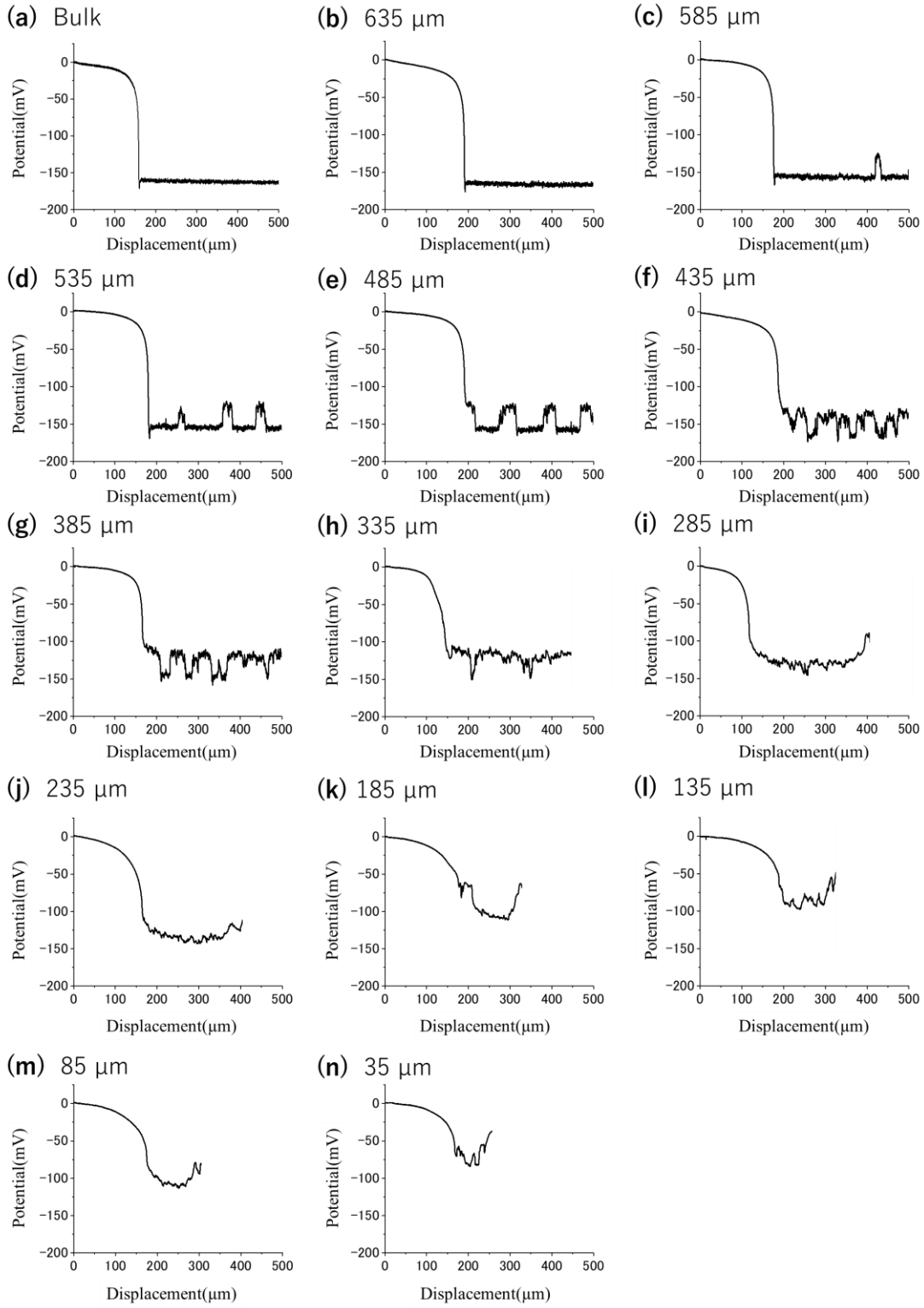

Fig. 6.4 Electric potential profiles for presentative positions in the damage zone and in bulk. The vertical axis represents the electric potential (mV), and the horizontal axis represents the distance advanced by the glass electrode (= displacement, μm). The potential profile covers

displacements up to 500 μm, and the absence of potential data in certain regions indicates that the glass electrode penetrated through the DN gel, resulting in the lack of data in those areas.

6.3.3 Calculate the polymer concentration distribution in the damage zone and convert polyelectrolyte structure to a color map

To gain detailed insights into the spatial distribution of the first network, I estimated the polymer concentration distribution of the first network from the electric potential distribution. Therefore, I converted the Donnan potential to the counter ion concentration distribution using the Donnan potential equation (6.1)[18].

$$\Phi = \frac{2.3RT}{zF} log \frac{\gamma_s C_s}{\gamma_g C_g} \qquad (6.1)$$

Here, Φ represents the Donnan potential, R represents gas constant, T is absolute temperature, z is ionic valence, F is Faraday constant, γ_s and γ_g are activity coefficient of counter-ions and C_g and C_s are molar concentration of counter-ions, in gel and in external solution, respectively. C_s equal to salt concentration in the external solution (10^{-5} M).The activity coefficient γ_s=1 for C_s =10^{-5} M. Since the first network is synthesized from 1:1 monomeric electrolyte, z =1, and the polyelectrolyte concentration distribution of the first network is the same to the counter-ion distribution C_g. In order to estimate C_g from Eq. 1 by using the measured Φ, I need to know γ_g, which can be obtained from Φ and C_g of the virgin DN gel or in the undamaged region. Using Φ = -163 mV (= the average electric potential in bulk) and C_g (=monomer concentration at preparation divided by swelling ratio), γ_g was then estimated approximately 0.16. This activity coefficient value is consistent with that of approximately 0.2 estimated by a different method[1,21]. In current technology, it is difficult to thoroughly evaluate the changes in activity coefficients associated with conformational changes of the first network. Therefore, in this experiment, regardless of the extent of the first network rupture, I assumed that the activity coefficient of counterions matches the bulk activity coefficient and calculated the polymer concentration.

With the known values of γ_s=1, γ_g=0.16, and Cs =10^{-5} M, the counter-ion concentration in the damage zone ($C_{\mathrm{g},d\mathrm{amage}}$), which represents the polyelectrolyte concentration, was calculated from the electric potential values using equation (6.1). Here, the activity coefficient value was assumed to be constant regardless of fracture and swelling.

The obtained polymer concentration distributions were expressed as a 24-gradation color map, from red color for maximum polymer concentration of 3.59×10^{-2} M to blue color for minimum polymer concentration of 4.81×10^{-4} M, with a gradation width of 1.48×10^{-3} M, as shown in Figure 6.5. In the color map, the horizontal axis represents the position from the crack tip and the vertical axis represents the depth from the gel surface. At each position, the depth of 0 μm was determined as the surface of the gel after equilibrium swelling. The maximum value of depth was set to 500 μm. In positions around the crack, the absence of the depth-wise color map indicates that data could not be acquired due to the glass electrode penetrating through the hydrogel.

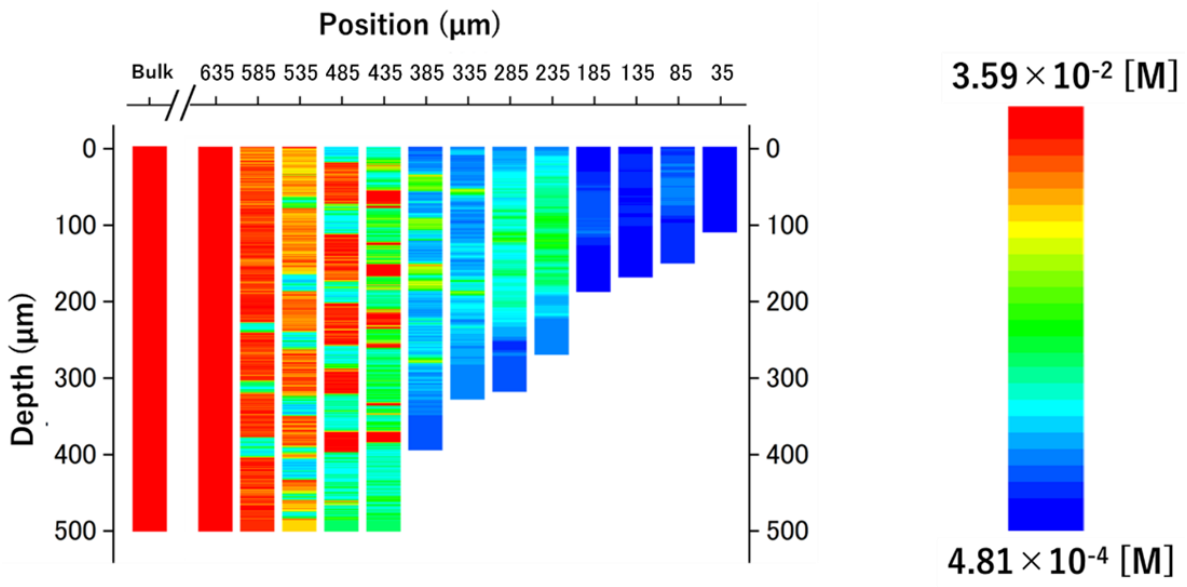

Figure 6.5. Color map of the polymer concentration distribution near the crack tip, where position is the distance from the crack tip along X-axis and depth is the distance from the gel surface along Z-axis. The correspondence between polymer concentration and color is shown in the legend.

6.3.4 Internal structure of polyelectrolyte network in the damage zone and fracture behavior during DN gel formation

In Figure 6.5 the thickness of the DN gel gradually decreases from the 385 μm position toward the crack tip (the 35 μm position). The undamage zone shows a red color at a distance of more than the 635 μm position from the crack tip. This indicates that, as seen in Figure 6.6 (i), the first network is not ruptured, and the polymer concentration of the first network remains high. In the damage zone, the polymer concentration is not uniform along Z-axis, and particularly, the polymer concentration is low at the hydrogel surfaces. This is because the damage to the hydrogel originates from the hydrogel surfaces. This shows that the destruction and necking[22] of the hydrogel progress from the surfaces of the gel, indicating that the damage is more significant compared to the interior of the gel. In the preyield zone from the 235 μm to 585 μm position, a two-step change can be observed approaching the crack tip. First, at the positions from 435 μm to 585 μm, which are close to the undamaged region, there is a coexistence of the red region representing the undamaged area and the low-concentration green region resulting from damage. As it approaches the crack tip, the proportion of the green region increases. At this point, it can be assumed that the first network is in a state similar to Figure 6.6 (ii). Furthermore, at the positions from 235 μm to 385 μm, closer to the crack tip, the red region representing the undamaged portion disappears, and the polymer concentration changes from green to blue throughout the depth of the gel. This indicates that the first network is becoming non-continuous and undergoing clustering, as shown in Figure 6.6 (iii) .In the subsequent yield zone from the 85 μm to 185 μm position near the crack tip, the green region also almost disappears, and the polymer concentration of the first network is significantly lower than in the preyield zone. At the 35 μm position, the color map is almost uniformly blue. Considering the spatial resolution of microelectrode technique is 800 nm, the first network in the yield zone is expected to consist of very fine clusters below the resolution size, as depicted

in Figure 6.6 (iv). Therefore, microelectrode technique measures the polymer concentration of the extensively ruptured first network clusters throughout the entire Z-axis, taking the average value. This polymer concentration indicates that it is approximately 1/100 compared to the bulk.

These results indicate that internal rupture of the first network in the Z-axis direction occurs when the DN gel is torn in the Y-axis direction, representing a successful observation of a phenomenon that was previously unmeasurable with conventional microscopy and scattering methods. Two factors are considered as reasons for internal rupture of the first network in the Z-axis direction. One is related to the density difference of the first network in the DN gel, and the other is related to the fracture surface formed during tearing.

Regarding the consideration of the first network in DN gel, I have three hypotheses. Firstly as shown in Figure 6.7 (a), it is conceivable that the spatial density difference of the first network immediately after the polymerization of the DN gel may lead to the formation of regions where the first network is preferentially ruptured and regions where it remains unruptured. When there is a difference in the density of the first network within the DN gel, the lower-density regions of the first network may undergo preferential rupture when subjected to the same strain. While this phenomenon has been previously observed in the stretching direction based on conventional measurement results[13,15,17], there is a possibility that a similar phenomenon occurs in the Z-axis direction as well. Secondly as shown in Figure 6.7 (b), in the consideration of the formation of the tearing surface, ideally, the vector of global strain would align with the tearing direction. However, due to the difficulty in highly controlling tearing behavior, there is a possibility that the true tearing surface is inclined from the XZ plane. Ideally, when tearing the DN gel in the Y-axis direction, in the preyield zone, regions of unruptured and ruptured areas would alternately appear along the Y-axis. It could be inferred that the extent of rupture of the first network in each region remains unchanged along the Z-axis. However, if the true tearing

surface is inclined from the XZ plane, regions of unruptured and ruptured areas would alternately appear along the normal vector direction of the tearing surface. As a result, it might appear that the extent of rupture of the first network varies along the Z-axis. Lastly as shown in Figure 6.7 (c), There is a possibility of a phenomenon resembling buckling occurring in the Z-axis direction at the tearing interface. When tearing the DN gel in the Y-axis direction, forces are applied in the direction of compression along the Z-axis, which may result in partial rupture of the first network inside the DN gel due to buckling-like phenomenon, leading to the formation of characteristic structures. This dissertation does not investigate these possibilities. Even after excluding these possibilities, tearing the hydrogel revealed spatial anisotropy in the first network rupture.

Additionally, based on the trend in polymer concentration changes from the color map, I inferred the internal rupture of the first network within the DN gel. In the preyield zone corresponding to positions from 235 μm to 585 μm, there is a low polymer concentration region spreading along the Z-axis. This suggests a phenomenon like local necking occurring in the Z-axis direction. Furthermore, in the yield zone corresponding to positions 35μm to 185μm, the first network becomes finely clustered throughout the entire Z-axis direction, representing a state typical of the global necking phenomenon observed during the general fracture of DN gels. These results represent the first measurement of the fracture pattern in the Z-axis direction of the DN gel and align with the trends in energy dissipation reported by Matsuda et al[14]. in the yield zone and preyield zone. Therefore, it is suggested that the toughening and energy dissipation during the fracture of the DN gel involve contributions from two necking phenomena: local necking, which may not appear as fracture at first glance, and global necking, which is observable optically.

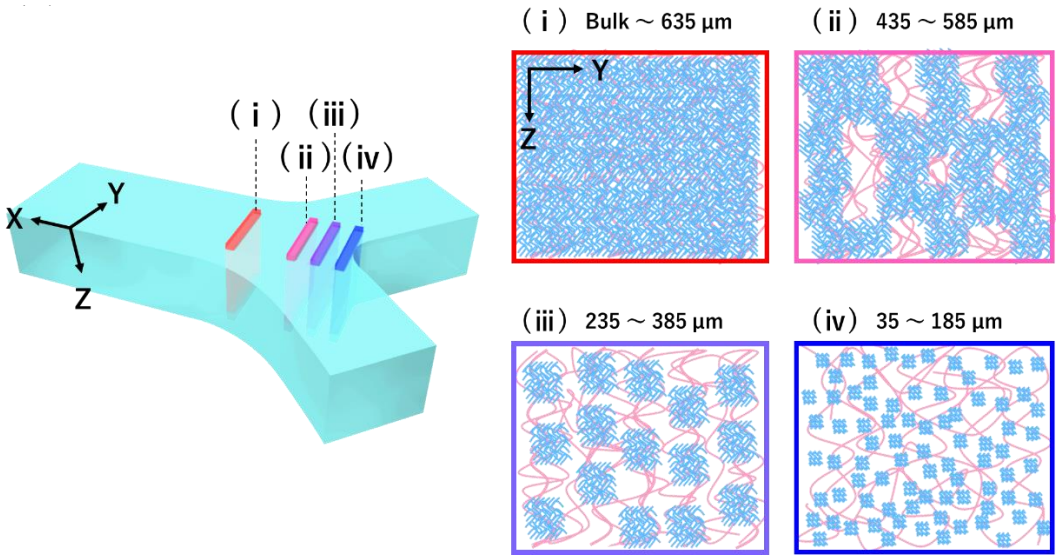

Fig. 6.6 Illustration of the fracture structure of DN gel in the Y-Z plane. The damage sustained by the tearing DN gel is shown in (i)-(iv) as in the legend of Figure 6.5, and the structure of the first network (blue) and second network (red) at each position is schematically illustrated.

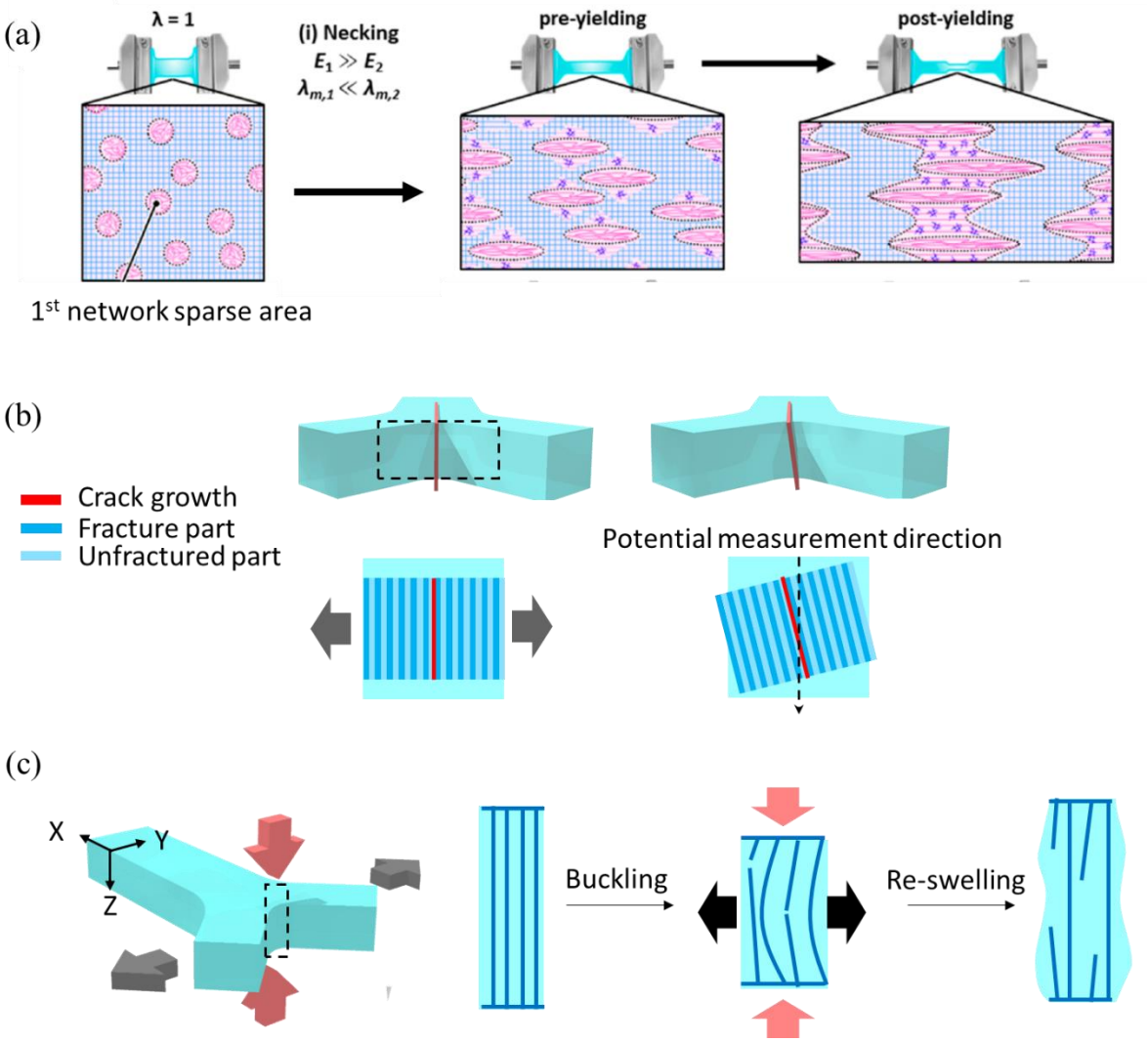

Fig. 6.7 The hypothesis about reasons that form distinctive structures in the preyield zone. (a) The sparsity or density of the potential 1st network[17]. (b) The direction of crack propagation plane is tilted from X-Z plane. (c) Buckling-like phenomenon.

6.4 Conclusion

Using the improved microelectrode technique, I successfully visualized the polymer concentration distribution of the first network (spatial distribution of the first network) in the damage zone of the DN gel by measuring the Donnan potential in the Z-axis direction. This result is a phenomenon that could not be confirmed by conventional microscopic measurements or scattering methods. As a result, it was revealed that the damage zone extends not only in the XY plane but also in the Z-axis direction by at least 500 μm or more, indicating different internal structures between preyield zone and yield zone. In the preyield zone corresponding to positions 235μm to 585μm, there is a structure where ruptured and unruptured parts of the first network alternate along the Z-axis, and a local necking phenomenon is observed, where the unruptured part decreases as it approaches the crack tip. It can be inferred that this phenomenon causes energy dissipation in the preyield zone. In the yield zone corresponding to positions 35μm to 185μm, it is inferred that the structure of the first network becomes finely homogeneous within the resolution range of microelectrode technique, leading to a global necking phenomenon. These results are the first spatial and quantitative demonstration of sub-micrometer structures in the damage zone of DN gels, which have been challenging to measure with conventional techniques.

The high sensitivity and spatial resolution of microelectrode technique makes it a novel and powerful approach for analyzing the internal structures of polyelectrolyte hydrogels with intricate architectures.

6.5 References

1. Nishimura, T.; Guo, H.; Kiyama, R.; Katsuyama, Y.; Gong, J.P.; Kurokawa, T. In Situ Evaluation of the Polymer Concentration Distribution of Microphase-Separated Polyelectrolyte Hydrogels by the Microelectrode Technique. *Macromolecules* **2021**, 54, 10776–10785.
2. Gong, J. P.; Katsuyama, Y.; Kurokawa, T.; Osada, Y. Double- Network Hydrogels with Extremely High Mechanical Strength. Adv. Mater. **2003**, 15, 1155−1158.
3. Yasuda, K.; Gong, J. P.; Katsuyama, Y.; Nakayama, A.; Tanabe, Y.; Kondo, E.; Ueno, M.; Osada, Y. Biomechanical Properties of High-Toughness Double Network Hydrogels. *Biomaterials* **2005**, *26* (21), 4468–4475.
4. Gong, J. P.; Kurokawa, T.; Narita, T.; Kagata, G.; Osada, Y.; Nishimura, G.; Kinjo, M. Synthesis of Hydrogels with Extremely Low Surface Friction. *Journal of the American Chemical Society* **2001**, pp 5582–5583.
5. Gong, J. P. Why are double network hydrogels so tough? *SoftMatter* **2010**, 6, 2583−2590.
6. Huang, X.; Li, J.; Luo, J.; Gao, Q; Mao, A.; Li, j. Research Progress on Double-network Hydrogels. *Mater. Today Commun.* **2021,** 29, 102757
7. Means ,A. K.; Shrode, C. S.; Whitney, L. V.; Ehrhardt, D. A.;Grunlan, M. A. Double Network Hydrogels That Mimicthe Modulus, Strength, and Lubricity of Cartilage. *Biomacromolecules* **2019**, 20(5), 2034−2042
8. Sun, J. Y.; Zhao, X.; Illeperuma, W. R. K.; Chaudhuri, O.; Oh,K. H.; Mooney, D. J.; Vlassak, J. J.; Suo, Z. Highly stretchable and tough hydrogels. *Nature* **2012**, 489, 133−136.

9. Tanaka, Y. A local damage model for anomalous high toughness of double-network gels. *Europhys. Lett.* **2007**, 78, No. 56005.

10. Brown, H. R. A model of the fracture of double network gels. *Macromolecules* **200**7, 40, 3815−3818.

11. Yu, Q. M.; Tanaka, Y.; Furukawa, H.; Kurokawa, T.; Gong, J. P. Direct observation of damage zone around crack tips in double network gels. *Macromolecules* **2009**, 42, 3852−3855.

12. Tanaka, Y.; Kawauchi, Y.; Kurokawa, T.; Furukawa, H.; Okajima, T.; Gong, J. P. Localized yielding around crack tips of double-network gels. *Macromol. Rapid Commun*. **2008**, 29, 1514−1520.

13. Liang, S.; Hu, J.; Wu, Z. L.; Kurokawa, T.; Gong, J. P. Toughness Enhancement and Stick-Slip Tearing of Double-Network Hydrogels in Poly(Ethylene Glycol) Solution. *Macromolecules* **2012**, 45, 4758−4763.

14. Matsuda, T.; Kawakami, R.; Nakajima, T.; Hane, Y.; Gong, J. P. Revisiting the Origins of the Fracture Energy of Tough Double Network Hydrogels with Quantitative Mechanochemical Characterization of the Damage Zone. Macromolecules 2021, 54, 10331−10339.

15. Liang, S.; Wu, Z. L.; Hu, J.; Kurokawa, T.; Yu, Q. M.; Gong, J.P. Direct observation on the surface fracture of ultrathin film double network hydrogels. *Macromolecules* **2011**, 44, 3016−3020.

16. Nakajima, T.; Kurokawa, T.; Ahmed, S.; Wu, W.-L.; Gong, J. P. Characterization of internal fracture process of double network hydrogels under uniaxial elongation. *Soft Matter* **2013**, 9, 1955−1966.

17. Fukao, K.; Nakajima, T.; Nonoyama, T.; Kurokawa, T.; Kawai, T.; Gong, J. P. Effect of relative strength of two networks on the internal fracture process of double network hydrogels as revealed by in situ small-angle X-ray scattering. *Macromolecules* **2020**, 53, 1154−1163.

18. Donnan, F. G. Theory of Membrane Equilibria and Membrane Potentials in the Presence of Non-Dialyzing Electrolytes. A Contribution to *Physical-Chemical Physiology* **1995**; Vol. 100.

19. Guo, H.; Kurokawa, T.; Takahata, M.; Hong, W.; Katsuyama, Y.; Luo, F.; Ahmed, J.; Nakajima, T.; Nonoyama, T.; Gong, J. P. Quantitative Observation of Electric Potential Distribution of Brittle Polyelectrolyte Hydrogels Using Microelectrode Technique. *Macromolecules* **2016**, *49* (8), 3100–3108.

20. Guo, H.; Hong, W.; Kurokawa, T.; Matsuda, T.; Wu, Z. L.; Nakajima, T.; Takahata, M.; Sun, T.; Rao, P.; Gong, J. P. Internal Damage Evolution in Double-Network Hydrogels Studied by Microelectrode Technique. *Macromolecules* **2019**, *52* (18), 7114–7122.

21. Nakajima, T.; Chida, T.; Mito, K.; Kurokawa, T.; Gong, J. P. Double-Network Gels as Polyelectrolyte Gels with Salt-Insensitive Swelling Properties. *Soft Matter* **2020**, *16* (23), 5487–5496.

22. Na, Y. H.; Tanaka, Y.; Kawauchi, Y.; Furukawa, H.; Sumiyoshi, T.; Gong, J. P.; Osada, Y. Necking Phenomenon of Double-Network Gels. *Macromolecules* **2006**, 39, 4641−4645.

Chapter 7 Summery

I refined the microelectrode technique to enhance spatial resolution and developed a method for spatial and in-situ measurement of the heterogeneous internal structure of the polymer network constituting polyelectrolyte hydrogels. Subsequently, I successfully conducted performance evaluations of the microelectrode technique and measured and visualized the internal structure of polyelectrolyte hydrogels with unknown heterogeneous structures.

In **Chapter 3**, I focused on improving the microelectrode technique. The conventional microelectrode technique lacked sufficient spatial resolution to accurately represent the polymer density distribution of polyelectrolyte hydrogels with heterogeneity. To address this limitation, I aimed to enhance spatial resolution by replacing equipment directly linked to the sensitivity improvement of the microelectrode technique and thoroughly blocking noise introduced from electromagnetic waves generated by other electronic devices, power cables, and similar sources. As a result, compared to the conventional measurement system, the effective number of samples increased approximately 38 times, and the standard deviation of white noise, one of the indicators of improved spatial resolution, was successfully reduced to about 1/6. Furthermore, this reduction confirmed the capability to detect polymer concentration changes on the 10^{-7} M scale, exceeding 2% in reference solution (10^{-5} M $NaCl_{aq}$).

In **Chapter 4**, I confirmed the extent to which the improved microelectrode technique can measure the scale of heterogeneous internal structures of polyelectrolyte hydrogels. I created a model hydrogel, P-DN gel, known for its heterogeneous structure on the μm scale, and measured electric potential of the P-DN gel. As a result, the electric potential profile exhibited a rectangular wave-like pattern, with alternating electric potential ranges representing the bulk

hydrogel and polyelectrolyte micro-particle hydrogels. The structural sizes obtained from the electric potential profile matched the average size measured for any arbitrary chord length of the polyelectrolyte micro-particle hydrogels. Furthermore, by creating 3D color mapping, I successfully revealed the spatial distribution of polyelectrolyte micro-particle hydrogels within P-DN. From the above, it is evident that the microelectrode technique is capable of spatially measuring μm-scale heterogeneous structures of polyelectrolyte hydrogels.

In **chapter 5**, to verify the utility of the improved microelectrode technique, I attempted structural measurements of polyelectrolyte hydrogels with irregular and unknown-scale heterogeneous internal structure, unlike P-DN. I conducted electric potential measurements and conversion to polymer concentration profiles using the microelectrode technique with a phase separated hydrogels having a structure where polyelectrolyte network undergoes phase separation. As a result, I successfully observed the spatial distribution of polyelectrolyte network separated into the dense phase and the sparse phase. Additionally, a trend in phase separation was observed, where the polymer concentration in the dense phase increased as the degree of phase separation intensified, while the polymer concentration in the sparse phase decreased. This is consistent with the observation results of polyelectrolyte network obtained through TEM. Furthermore, from the concentration changes between the dense and sparse phases in the polymer concentration profile, it was determined that the microelectrode technique has a spatial resolution of at least 0.8 μm.

In **Chapter 6**, the purpose was to utilize the improved microelectrode technique to infer the fracture behavior based on the concept of the "sacrificial bond principle." This is crucial for

discussing the high-strength properties of DN gel. To achieve this, DN gel was partially torn, and a spatial evaluation of the internal structure, including the damage zone, was conducted. Specifically, the electrical potential of the damaged zone formed by tearing the DN gel was measured at regular intervals from the crack tip. This revealed, for the first time, that the damage extends more extensively and spatially than the damage zones traditionally observed optically in DN gels. Additionally, there was success in visualizing the polymer concentration distribution of the first network (polyelectrolyte network) within the damage zone. Furthermore, in distinct yield zones and preyield zones with varying degrees of damage, different fracture behaviors were observed in the scanning direction of the microelectrode technique. (1) In the preyield zone: The first network undergoes local necking phenomenon, causing a separation between the fractured and unfractured parts. (2) In the yield zone: The first network undergoes global necking phenomenon, resulting in overall fracture. These results demonstrate, from a perspective of polymers structure, that the two-stage energy dissipation in the damage zone contributes to the toughening of DN gel.

The microelectrode technique offers an innovative and powerful approach as it eliminates the need for pre-treatments such as freeze-drying or staining for polyelectrolyte hydrogels. It enables the measurement of the internal structure and polymer concentration of polyelectrolyte hydrogels with sub-μm-scale heterogeneity. I expect that this method can be utilized in the design, characterization, and degradation assessment of functional polyelectrolyte hydrogels.

Accomplishments

Original papers (Related to doctoral dissertation)

1. **Nishimura, T.**; Guo, H.; Kiyama, R.; Katsuyama, Y.; Gong, J.P.; Kurokawa, T. In Situ Evaluation of the Polymer Concentration Distribution of Microphase-Separated Polyelectrolyte Hydrogels by the Microelectrode Technique. *Macromolecules* **2021**, 54, 10776–10785.

2. **Nishimura, T.**; Guo, H.; Katsuyama, Y.; Yoshida, M.; Gong, J.P.; Kurokawa, T. A Spatial Analysis of the Damage Zone in Double Network Hydrogel Using Microelectrode Technique. *Macromolecules* **2024**, online.

Original papers (Others)

1. Satoshi Tanikawa, Yuki Ebisu, Tomáš Sedlačík, Shingo Semba, Takayuki Nonoyama, Takayuki Kurokawa, Akira Hirota, Taiga Takahashi, Kazushi Yamaguchi, Masamichi Imajo, Hinako Kato, **Takuya Nishimura**, Zen-ichi Tanei, Masumi Tsuda, Tomomi Nemoto, Jian Ping Gong & Shinya Tanaka. Engineering of an electrically charged hydrogel implanted into a traumatic brain injury model for stepwise neuronal tissue reconstruction. *Scientific Reports* **2023**, 13, Article number.2233.

Conference (Related to doctoral dissertation)

(1) 西村 拓哉、郭 宏磊、黒川 孝幸、龔 剣萍：「微小電極法による DN ゲル内部構造のその場評価」

第 68 回高分子学会年次大会（令和 1 年 5 月，大阪）

(2) 西村 拓哉、郭 宏磊、黒川 孝幸、龔 剣萍：「微小電極法による電解質ゲル内部構造のその場評価」

日本分析化学会第 68 年会（令和 1 年 9 月，千葉）

(3) 西村 拓哉、郭 宏磊、黒川 孝幸、龔 剣萍：招待講演「微小電極法による DN ゲル内部構造のその場評価」

第 28 回ポリマー材料フォーラム（令和 1 年 11 月，名古屋）

(4) 西村 拓哉、郭 宏磊、黒川 孝幸、龔 剣萍：「微小電極法による電解質ゲル内部構造のその場評価」

2020 年繊維学会年次大会（令和 2 年 6 月，東京）

(5) 西村 拓哉、郭 宏磊、黒川 孝幸、龔 剣萍：「微小電極挿入による電解質ゲル内部の不均質構造のその場評価」

第 10 回 CSJ 化学フェスタ大会（令和 2 年 10 月，オンライン）

(6) 西村 拓哉、郭 宏磊、木山 竜二、龔 剣萍、黒川 孝幸：「電解質ミクロ相分離ゲル内部の局所ポリマー濃度計測法の構築」

第 11 回 CSJ 化学フェスタ大会（令和 3 年 10 月，オンライン）

(7) Takuya Nishimura; Honglei Guo; Ryuji Kiyama; Yoshinori Katsuyama; Jian Ping Gong; Takayuki Kurokawa：「A New Method to Measure the Internal Structure and Charge density of Polyelectrolyte Hydrogels.」

Polysolvat13（令和 3 年 11 月，オンライン）

(8) 西村 拓哉、郭 宏磊、木山 竜二、龔 剣萍、黒川 孝幸：「電解質ハイドロゲル内の局所的な内部構造や定量的なポリマー濃度の新規計測法」

第 31 回 MRS-J 年次大会（令和 3 年 12 月，オンライン）

(9) 西村 拓哉、郭 宏磊、水谷 晴香、椎村 響、龔 剣萍、黒川 孝幸：「局所ドナン電位測定を用いた電解質ハイドロゲル内のポリマーネットワーク構造解析」

第 72 回ネットワークポリマー講演討論会（令和 5 年 10 月，神奈川）

Conference (Others)

(10) 西村 拓哉 、郭 宏磊、黒川 孝幸、木山竜二、龔 剣萍：「微小電極法による電解質網目構造のその場観察」

高分子学会若手研究会 (平成 30 年 8 月，北海道）

(11) 西村 拓哉 、郭 宏磊、黒川 孝幸、木山竜二、龔 剣萍：「微小電極法による電解質網目構造のその場観察」

ゲルワークショップ イン 札幌 (平成 30 年 9 月，北海道）

Acknowledgement

This research on this dissertation has been carried out in the Laboratory of Transformational Soft Matter (TSM) and Laboratory of Soft and Wet Matter (LSW), Graduate School of Life Science, Hokkaido University, Japan, supervised by Professor Takayuki Kurokawa. Associate examiners are Professor Jian Ping Gong, Assistant Professor Tasuku Nakajima and Assistant Professor Takashi Kikukawa.

Firstly, I greatly appreciate all the support and encouragement of my respected supervisor, Professor Takayuki Kurokawa during my bachelor's, master's study in LSW and doctoral study in TSM. He gave me not only his tremendous academic support to be an outstanding researcher but also so many opportunities to relax through daily chat and board games . I really appreciate that he evaluated my doctoral research, and through a lot of discussions with him, I could acquire a deep understanding of polymer materials and an ability to analysis unknown data. I deeply respect his amicable personality, positive attitude and research understanding and considering.

I would like to many thanks also to TSM and LSW teachers, Professor Jian Ping Gong, Associate Professor Tasuku Nakajima, Assistant Professor Takayuki Nonoyama, Assistant Professor Daniel R. King for their helpful scientific comments, fruitful discussions and useful suggestions regarding my research. Additionally, Professor Jian Ping Gong provides various excellent insights and advice on research and paper, and furthermore, she carries an aura of dignity as a prominent researcher active in the world, which I deeply respect.

I would like to say a very big thank you to Associate Professor Guo Honglei in Sun Yat-sen University and Assistant Professor Takashi Kikukawa in Hokkaido University for the kind support on my experiment. Associate Professor Guo Honglei patiently taught me the Donnan potential measurement method and data analysis techniques until I could understand them. I am extremely grateful to him, as I believe my research would not have been possible without his support. Assistant Professor Takashi Kikukawa provided me with the opportunity to pursue a doctoral course. By entering the doctoral program, I not only experienced an enhancement in my academic abilities but also felt personal growth from within. I am truly grateful to him for providing me with this opportunity.

I am also very grateful to post-doctoral fellows, guest researcher and research assistants in “LSW and TSM.” Especially, Dr. Yoshinori Katsuyama provided me with many opportunities to "grow as a person," not only by offering a lot of advice and technical support for my research, but also by listening to and giving advice on everyday life concerns. I respect him very much. Also, Ms. Yukiko Hane and Ms. Miyuki Matsumoto help me on many occasions and I really appreciate their support.

I also would like to thank the staffs in TSM and LSW : Ms. Yuri Kamada, Ms. Saeko Iseya, Ms. Eiko Hasegawa, Ms. Yuki Okubo, Ms. Yumi Segawa and for helping me in financial works and lab life of Hokkaido University. Of course, I greatly appreciate all the past and present Japanese and International students of TSM and LSW for their kind and friendly attitude.

I want to gratefully acknowledge Hokkaido University’s “DX Doctoral Fellowship” supported by JSPS. It was impossible to complete my doctoral research without their financial support and fruitful opportunity.

Finally, special thanks to my family for all the support and encouragement during the life in Hokkaido University. I dedicate this dissertation to them.

Takuya Nishimura

Laboratory of Transformational Soft Matter

Graduate School of Life Science

Hokkaido University

Sapporo Japan

March 2024